https://doi.org/10.5194/egusphere-2026-4729
Preprint. Discussion started: 31 August 2026

Limited modelled legacy effects of drought on carbon and water fluxes in a temperate oak forest despite hydraulic impairment

J. Cale Baguley[1], Tristin Quaife[2], Lucy Rowland[3], Patrick Meir[4], Michael C. Bell[5], Manon E. B. Sabot[6], and Martin G. De Kauwe[1]

[1]School of Biological Sciences, University of Bristol, 24 Tyndall Avenue, Bristol BS8 1TQ, UK
[2]National Centre for Earth Observation, Department of Meteorology, University of Reading, Reading, United Kingdom
[3]Faculty of Environment, Science and Economy, University of Exeter, Exeter, UK.
[4]School of GeoSciences, University of Edinburgh, King's Buildings, Alexander Crum Brown Rd, Edinburgh, EH9 3FF, UK
[5]Centre for Sustainable Forestry and Climate Change, Forest Research, Alice Holt Lodge, Farnham, Surrey, UK
[6]Max Planck Institute for Biogeochemistry, Jena, 07745, Germany

Correspondence: J. Cale Baguley (calebaguley@btinternet.com)

Abstract. The projected increase in the intensity, frequency and duration of summer drought extremes under climate change poses a growing risk to forest ecosystems, even in mesic regions such as the UK. To accurately predict the impact of future summer droughts, it is necessary to account for both their immediate and legacy effects, as well as their influence on ecosystem sensitivity to drought over time. We introduce a stomatal optimisation scheme, Profit-Max, within the Joint UK Land Environment Simulator (JULES) land surface model (LSM) to improve predictions of plant response to drought induced water stress. We further extend the model to represent drought legacy effects through two approaches to capture hydraulic impairment of xylem. We evaluate these developments by simulating an old growth oak forest at the Alice Holt site in southern England during the 2022 UK summer (July to September), when rainfall was substantially below average (77mm of rainfall compared with a 1999-2018 median of 140mm) and national temperatures exceeded $40°$C for the first time. During the 2022 drought year, the stomatal optimisation scheme predicted reductions in annual GPP and LE, -26% and -33% respectively, relative to an average year (2011-2017). This was larger than the measured reduction in LE of -6%. The hydraulic legacy schemes simulated percentage loss of conductance of 9% to 40% ,with a carry-over effect on LE flux (-1% to -11%). We further explored ecosystem responses under more extreme future summers, including zero rainfall in spring (similar to the meteorology conditions of 2025) and a 50% reduction in rainfall over the remainder of the year. Despite substantial increases in the percentage loss of conductance (10% to 55%), the simulated reductions in GPP and LE remained modest in 2023, consistent with observations. The magnitude of these legacy effects, however, was sensitive to the representation of hydraulic impairment and recovery. Overall, our results demonstrate the feasibility of representing drought legacy effects within a LSM and highlight the importance of hydraulic impairment assumptions in shaping projected ecosystem responses to extreme drought. While the simulations suggest limited legacy impacts on carbon uptake and latent heat fluxes at Alice Holt following the 2022 drought, evaluation of the underlying plant water status and hydraulic function will require independent observations of water potential and hydraulic function across the soil-plant-atmosphere continuum, as flux tower data alone may not fully constrain longer-term impacts on growth and resilience.

https://doi.org/10.5194/egusphere-2026-4729
Preprint. Discussion started: 31 August 2026

1 Introduction

Climate change is increasing the frequency, intensity and duration of drought events, driving widespread forest mortality across the globe (Hammond et al., 2022), including in temperate mesic systems such as European oak stands (Gentilesca et al., 2017). The effects of these changes in drought regimes are further amplified by the increasing co-occurrence of heatwaves, which exacerbate plant water stress, and give rise to so-called "hot droughts", where elevated atmospheric evaporative demand combined with depleted soil moisture substantially intensifies system stress and increases the risk of tree mortality (Adams et al., 2017; McDowell et al., 2022). In recent decades, Europe has experienced several record-breaking extreme hot and dry summers (e.g. 2003, 2005, 2018, 2022, 2024 and 2025), leading to marked reductions in ecosystem productivity (Ciais et al., 2005; Bastos et al., 2020), increased wildfire activity (Dupuy et al., 2019), and and broader disruptions to ecosystem structure, functioning and health (Knutzen et al., 2025).

The shift towards more frequent compound heat-drought events means that summer atmospheric and climatic extremes can no longer be viewed as independent events (Ogle et al., 2015; Werner et al., 2025). Furthermore, forest ecosystems are increasingly exposed to new extreme events before having fully recovered from the previous disturbances (Schwalm et al., 2017; Seneviratne and Ciais, 2017). Predicting the resilience of forest ecosystems to future climate extremes thus requires understanding the degree to which ecosystems remain conditioned by prior drought and heat exposure, including both short-term seasonal legacies and longer-term multiyear legacy effects.

Forest responses to drought are complex and manifest across a wide range of timescales, giving rise to persistent legacy effects. During drought events, forests often exhibit immediate declines in gross primary productivity (GPP) (Shao et al., 2024), alongside reductions in transpiration (Sulman et al., 2016; Sinacore et al., 2019) and leaf area (Martin-StPaul et al., 2013; Wolfe et al., 2016) that typically recover within a couple of growing seasons. Legacy effects in ecosystem-scale carbon uptake derived from eddy covariance observations are often weak or short-lived (Yu et al., 2017; Schwalm et al., 2017; Kannenberg et al., 2019), implying that physiological processes that were downregulated during drought stress recover rapidly (Ruehr et al., 2019). In contrast, reductions in radial stem growth inferred from tree rings can persist for more than five years following a drought event (Anderegg et al., 2016), due to shifts in carbon allocation to and leaf and root recovery (Ogaya and Penuelas, 2006; Rao et al., 2026).

Yet, our understanding of how drought legacy effects persist and influence recovery and subsequent future response to drought remains incomplete. Increasing empirical evidence demonstrates that the impacts of severe drought can persist for months to years beyond the recovery of meteorological conditions, with consequences for growth, mortality risk, hydraulic function, and community composition (Anderegg et al., 2012; Ogle et al., 2015; Anderegg et al., 2020). These drought legacy effects can modify ecosystem sensitivity to subsequent climate extremes, potentially amplifying or dampening future responses and contributing to nonlinear dynamics and threshold behaviour that are difficult to predict from immediate drought responses alone (Reyer et al., 2015). Despite growing recognition of their ecological significance, the mechanisms controlling the magnitude, persistence, and spatial variability of drought legacies remain poorly understood.

https://doi.org/10.5194/egusphere-2026-4729
Preprint. Discussion started: 31 August 2026

On the one hand, most experimental studies have focused either on the direct impact of drought, or on relatively shorter-term manipulations (Ruehr et al., 2019). On the other hand, whilst observation networks such as FLUXNET (Baldocchi et al., 2001) provide valuable insight into the multi-year time course of forest surface fluxes, direct comparison between drought events across both time and space is complicated by large differences in the conditions prior to drought, the severity of the drought event, species responses and the meteorological conditions during recovery. Consequently, it remains challenging to develop and test mechanistic theories of drought legacies and their representation in ecosystem models, limiting our ability to predict forest resilience under increasingly frequent and severe summer droughts.

Land Surface Models (LSMs) provide a key framework for quantifying the response of terrestrial ecosystems to meteorological forcing, representing coupled exchanges of energy, water, and carbon between vegetation, soils, and the atmosphere. However, many LSMs have historically struggled to represent both the magnitude and persistence of drought impacts, often simulating an overly rapid decline in carbon uptake during drought while failing to capture longer-term legacy effects that persiste after environment conditions recover (Huang et al., 2016; Ukkola et al., 2016; Kolus et al., 2019). Recent developments have incorporated more mechanist representations of plant hydraulics, in some cases coupled with stomatal optimisation approaches (see Sabot et al., 2022a), to improve the representation of plant responses to water stress (Eller et al., 2020; Kennedy et al., 2019; De Kauwe et al., 2022; Alléon et al., 2025). These approaches have substantially improved simulations of GPP and latent heat (LE) during drought events (De Kauwe et al., 2020a).

One key process underlying drought legacy is the long-term impairment of xylem hydraulic transport capacity by embolisms formation, which reduces whole-plant hydraulic conductivity and is a major contributor to drought-induced plant mortality (McDowell et al., 2008; Anderegg et al., 2012). However, directly linking plant mortality to the passing of a specific hydraulic threshold remains difficult with additional factors, such as defoliating insect outbreaks, contributing to drought-induced mortality (Anderegg et al., 2015). Several hydraulic impairment approaches have been developed to represent these hydraulic legacy effects in ecosystem models. Those can broadly be grouped according to how hydraulic damage is represented and whether recovery is allowed.

Existing modelling approaches to hydraulic drought legacies broadly fall into two categories. A first set of approaches represents hydraulic impairment as a reversible or partially reversible shift in vulnerability to water stress. For example, Mackay et al. (2015) reduced hydraulic conductivity as a function of predawn water potentials, allowing for daily recovery, effectively modifying the shape and maximum of the hydraulic vulnerability curve. Similarly, Lu et al. (2020) constrained hydraulic conductance based on the historic minimum water potential over a reference time window varying from daily to seasonal (see Sabot et al., 2022b, for a practical test of this time window), with fractional recovery occurring when water potentials become less negative. Yao et al. (2025) adopted a related approach by constraining recovery of both hydraulic conductance and an empirical drought stress factor following drought. Although these models differ in implementation, they all assume hydraulic impacts can recover, at least partially, following the alleviation of water stress.

A second group of models assumes that drought induces more persistent, irreversible damage. Ruffault et al. (2022) and (Paschalis et al., 2024) modelled embolism as a largely irreversible loss of hydraulic conductance, with recovery occurring only through the production of new xylem tissue in the latter model. Such formulations allow stronger and longer-lasting

https://doi.org/10.5194/egusphere-2026-4729
Preprint. Discussion started: 31 August 2026

legacy effects, including the emergence of hydraulic mortality thresholds, and are more consistent with the view that embolism removal is limited and that recovery commonly requires xylem turnover rather than rapid repair processes.

Despite these developments, uncertainty remains regarding the physiological mechanisms underlying hydraulic recovery and drought legacies. Recent evidence suggests that hydraulic safety traits exhibit only limited plasticity across environmental conditions, raising questions about model formulations that represent drought legacies through shifts in vulnerability characteristics or hydraulic safety thresholds (Ramírez-Valiente et al., 2025). Likewise, empirical support for widespread refilling of embolised xylem remains limited, and the extent to which embolism can be routinely repaired under tension is still debated. An alternative and increasingly explored view is that recovery of hydraulic function occurs primarily through the production of new conductive tissue, with embolised xylem persisting until it is replaced through xylem turnover (Deans et al., 2026). If so, drought-induced hydraulic damage may be considerably more persistent than assumed in models that permit rapid recovery of conductance following rewetting. These findings highlight the need for closer alignment between model assumptions and the emerging empirical understanding of hydraulic legacies.

Here, we implement the stomatal optimisation scheme (Profit-Max) of Sperry et al. (2017) within the JULES (Joint UK Land Environment Simulator) LSM (Clark et al., 2011). Building on this framework, we then develop and implement two alternative models of hydraulic impairment to capture the long-term legacy effects of drought stress on a tree's hydraulic transport capacity. The first model, termed "k_{max}-impaired", extends the framework of Mackay et al. (2015) by assuming that that xylem conductance declines progressively as a function of a tree's instantaneous hydraulic state. In contrast, the second approach, termed "Trunk-impaired", assumes that hydraulic damage occurs instantaneously and cannot be recovered. This formulation additionally accounts for vertical variations in hydraulic impairment along the unsegmented tree trunk due to increasingly negative water potentials when moving up the trunk.

We evaluate model predictions against eddy-covariance observations from the Alice Holt old-growth oak Forest in southern England during the extreme 2022 summer drought (Tripathy and Mishra, 2023). Specifically, we quantify both the immediate reduction in ecosystem-scale fluxes during 2022 and the legacy effects on fluxes during 2023. We then use the model to explore a range of more severe drought scenarios representative of future UK climate extremes for the region, examining how different representations of hydraulic impairment alter projected tree resilience. We hypothesise that the relatively high hydraulic resistance to stress of the site's oaks will buffer against hydraulic failure under moderate drought events experienced in the UK. Consequently, we expect larger legacy effects to emerge primarily through cumulative reductions in hydraulic conductance, rather than irreversible loss of function during a single drought event.

2 Methods

2.1 Alice Holt site

Located in southern England ($51^\circ\ 07^{'}$ N, $0^\circ\ 51^{'}$ W), Alice Holt is a research forest managed by Forest Research. Between 1971 and 2000, Alice Holt experienced a mean annual average temperature of $10°$C (annual range: $-0.5°$C to $22.5°$C) and a mean annual average rainfall of 800mm. As part of a long-term carbon dioxide flux monitoring initiative, an eddy- covariance tower

https://doi.org/10.5194/egusphere-2026-4729
Preprint. Discussion started: 31 August 2026

began continuous observation of an enclosure called "the Straits" inclosure in 1998 (Wilkinson et al., 2012). The 90-hectare Straits enclosure is primarily composed of oak (*Quercus robur*), with a smaller area of mixed conifers, including Corsican pine (*Pinus nigra subsp laricio Maire*) and Scots pine (*Pinus sylvestris L.*) The understory is dominated by hazel (*Corylus avellana L.*) and hawthorn (*Crataegus monogyna Jacq.*).

The stands are managed as a commercial oak woodland with the eastern and western halves thinned in 2007 and 2015, respectively. The site was also impacted by a severesever defoliation event linked to moth caterpillars in 2009 and 2010, leading to a reduction in observed GPP (Wilkinson et al. 2012), which was subsequently recovered in 2011. To to avoid these defoliation events impacting our simulations,this we limited the eddy-covarianceflux data used to evaluate the model to the period 2011 to 2017 inclusive, and to the year 2022. We note that the data for the period 2018 to 2021 was not available at the time of writing.

A leaf area index (LAI) climatology for Alice Holt was constructed from MODIS LAI data (Myneni et al., 2021) covering the period 1999-01-01 to 2020-01-01, as described in appendix A.

Volumetric soil water content at the site was measured half-hourly using the time-domain measurement method for the period 2022 to 2023. Measurements from CS616 sensors are collected and stored on a CR3000 datalogger (both Campbell Scientific, Shepshed, UK). Aditional volumetric soil water content measurements for the site were obtained from the Cosmic-ray soil moisture monitoring network UK data base (Cooper et al., 2021). Observations of atmospheric CO2 concentration were obtained from the Mauna Loa CO2 records (Mauna Loa Observatory).

2.2 2022 UK summer drought

The UK summer of 2022 was one of the hottest and driest on record in the UK. With an average maximum daily temperature of 20°C, it ranks as the third-warmest summer of the last 20 years (Hollis et al., 2019) and, at the time, included the highest temperature ever recorded in the UK, 40.3°C (recorded on July 19th in Coningsby, Lincolnshire). It was also exceptionally dry, with total summer rainfall averaging 161 mm across the UK, compared with 264 mm for summers from 2006 to 2025.

The Alice Holt site experienced similar extreme conditions to the wider UK during the summer of 2022. Mean daily maximum temperature was 23°C (Fig 1a), and the cumulative rainfall for the summer of 2022 was substantially lower than the average for the period 2011 to 2017, that is, 77 mm compared with 140 mm. This marked reduction in rainfall started in April/May, with the rainfall starting to recover after September (Fig 1b). Consequently the cumulative climactic water deficit for 2022 reached was higher than the average for the period 2011 to 2017, 300 mm compared with 2 mm(Fig 1d).

2.3 2023 post drought year

2023 in the UK was characterised by the driest February in 30 years followed by the sixth wettest March on record. Summer temperatures peaked in June at 32°C, below 2022's peak of 40.3°C. Over the summer Alice Holt experienced a mean daily maximum temperature of 21°C, 2 ∘ C lower than 2022. Alice Holt recorded a total summer rainfall of 164mm, higher than the average 140mm.

https://doi.org/10.5194/egusphere-2026-4729
Preprint. Discussion started: 31 August 2026

2.4 Model description

The Joint UK Land Environment Simulator (JULES; Best et al., 2011; Clark et al., 2011) is a community LSM that simulates the exchange of carbon, water, energy, and momentum between the land surface and atmosphere. JULES can be run as both a stand-alone model or as the land surface scheme within the Met Office's Unified Model (a weather and climate model).

In this study, we use JULES version 7.4 as a stand-alone model. Briefly, all simulations used the "big leaf" canopy scheme (Clark et al., 2011) to scale leaf-level carbon and water fluxes to the canopy. Photosynthesis in C3 plants follows the Farquhar, von Caemmerer, and Berry model (Farquhar et al., 1980), where assimilation is determined by the minimum of three limiting rates; RuBisCO-limited, electron transport-limited, and triose phosphate utilisation-limited. In the default model configuration ("CRTL"), stomatal conductance is represented using the semi-empirical stomatal modelformulation of MEDLYN et al. (2011), with photosynthetic capacity down regulated as soil moisture declines. Soil water and heat fluxes are solved using the Richards equation across six soil layers. Based on site information, total root depth was set to 1.0m and divided into six layers (0.05, 0.074, 0.11, 0.163, 0.242, and 0.361 m in order from the top to bottom layers) to capture subsurface hydrological dynamics.

Biogeochemistry (e.g., nitrogen and phosphorus cycling; Nakhavali et al., 2020) and dynamic vegetation schemes (Argles et al. e.g., REDD 2020, Cox TRIFFID 2001), were not included in the model configuration used here. Comprehensive model details for the CTRL model are provided in Best et al. (2011) and Clark et al. (2011).

To simulate the Alice Holt site, we represent the vegetation as a pure oak stand (*Quercus robur*), based on the dominant tree cover. As JULES does not include an explicit oak PFT, we used the broadleaf tree PFT as the basis for the simulation, assigning it a fractional cover of 1.0 to represent a pure oak stand (*Quercus robur*). V_{cmax} (μmol m$^{-2}s-2$) was estimated based on KATTGE et al. (2009) using foliar N concentrations in area basis based on an intercept ($v_{int} = 3.9$ Harper et al., 2016), a slope ($v_{sl} = 47.62$) and a leaf mass per area of 67.6 (Glopnet Quercus Robur average; Wright et al., 2005).

Carboxylation capacity at the reference temperature of 25°C is calculated as in KATTGE et al. (2009), with a leaf mass area of 67.6 g m^{-2}, an intercept and a vsl of 47.62 CO_2 m^{-2} s^{-1} We embedded a representation of plant hydraulics and two stomatal optimisation models as alternatives to the CTRL (see below), which we parameterised using P50 and P88 traits (the water potentials at which the xylem conductance reduces by 50% and 88%, respectively) for Quercus robur, -4.74MPa and -5.51MPa respectively (Lobo et al., 2018). For the Profit-Max and legacy impairment models, k_{max} was calibrated to 0.5×10^{-3}mol $^{-2}$ s^{-1} MPa^{-1} by visually fitting the modelled GPP and LE to observed values over the period 2011 to 2017, with the same k_{max} applied across both the stomatal optimisation and legacy impairment configurations.

2.4.1 Hydraulics and stomatal optimisation implementation

To improve the representation of the short-term response of trees to drought induced water stress, we implemented a simplified version of the Profit-Max optimisation scheme (ProfitMax Sperry et al., 2017) in JULES, consistent with the formulation used in the CABLE LSM (Sabot et al., 2020; De Kauwe et al., 2022).

Stomatal optimization models hypothesise that plants regulate their gas exchange and all relevant biophysical variables, for example, stomatal conductance, leaf water potential (ψ_l; MPa), and intercellular CO2 concentration, on an instantaneous basis

https://doi.org/10.5194/egusphere-2026-4729
Preprint. Discussion started: 31 August 2026

(i.e. each model timestep) by balancing marginal carbon gain ($\mathrm{CG}(\psi_l)$; unitless) against hydraulic cost ($\mathrm{HC}(\psi_l)$; unitless) to maximise net profit. The Profit-Max model defines profit as:

$$\mathrm{Profit}(\psi_l) = \mathrm{CG}(\psi_l) - \mathrm{HC}(\psi_l) \tag{1}$$

Carbon gain is defined as the net carbon dioxide (CO_2) assimilation (A_n; mol m^{-2} s^{-1}) rate at a given ψ_l normalised by the maximum assimilation rate achievable for fully open stomata under the prevailing environmental conditions:

$$\mathrm{CG}(\psi_l) = \frac{\mathrm{A}_n(\psi_l)}{\max(\mathrm{A}_n(\psi_l))} \tag{2}$$

The hydraulic cost function is given by:

$$\mathrm{HC}(\psi_l) = \frac{k(\psi_s) - k(\psi_l)}{k(\psi_s) - k_{crit}} \tag{3}$$

where $k(\psi_s)$ is the maximum plant hydraulic conductance (mmol m^{-2} s^{-1} MPa^{-1}) achieved at the current soil water potential (ψ_s; MPa), k_{crit} is the critical hydraulic conductance (mmol m^{-2} s^{-1} MPa^{-1}) that characterised hydraulic failure, (set to 5% of the maximum hydraulic conductance) (Brodribb and Cochard, 2008; Sabot et al., 2020) and $k(\psi_l)$ (mmol m^{-2} s^{-1} MPa^{-1}) is the hydraulic conductance at the ψ_l (MPa).

The plant hydraulic conductance for a given water potential (either the ψ_l, or the ψ_s) is modeled by a cumulative Weibul distribution:

$$k(\psi) = k_{max} e^{-\left(\frac{\psi}{b}\right)^c} \tag{4}$$

where k_{max} is the maximum hydraulic conductance (mmol m^{-2} s^{-1} MPa^{-1}), reached when $\psi = 0$.

Unlike (Sperry et al. (2017), who calculate profit for a range of uniformly sampled ψ_l, our implementation calculates profit for a range of uniformly sampled intercellular CO_2 concentrations ($n = 1000$). This reduces the computation time by avoiding the need to co-optimise the intercellular CO_2 concentration and stomatal conductance as described by in (De Kauwe et al., 2022). The calculation of ψ_l from the transpiration rate differs from the implementation in CABLE (De Kauwe et al., 2022) as we solve for ψ_l using a Newton Raphson approximation (see appendix C). The optimal leaf state is identified by selecting the intercellular CO_2 concentration with the greatest profit (equation 1).

2.4.2 Soil to root conductance model

To obtain a representative value of the root-zone, ψ_s, we calculate a weighted average of the water potential over N soil layers (see De Kauwe et al., 2015);

https://doi.org/10.5194/egusphere-2026-4729
Preprint. Discussion started: 31 August 2026

$$\psi_s = \frac{\sum_{i=1}^{N} w_i \psi_{si}}{\sum_{i=1}^{N} w_i} \tag{5}$$

where ψ_{si} is the water potential in the ith soil layer, and w_i the weighting of the ith soil layer. The weighting, w_i, for each soil layer is calculated as the water uptake from the ith soil layer if the root zone water potential is equal to the roots critical water potential ($\psi_{s\,crit}$; MPa).

$$w_i = (\psi_{si} - \psi_{s\,crit}) k_i \tag{6}$$

Where k_{si} (mmol m^{-2} s^{-1} MPa^{-1}) is the conductance between the soil and the root in the ith soil layer calculated following (Bonan et al., 2014). We note that the minimum weight, w_i, for any soil layer is set to 10^{-9} and ψ_s is set to $\psi_{s\,crit}$ when $\psi_{si} < \psi_{s\,crit}$ to prevent negative weights. $\psi_{s\,crit}$ was set to -3MPa. for this work. This approach places greater emphasis on water potential in the upper soil layers when the root zone is moist but progressively shifts weighting to deeper layers as drying occurs and hydraulic resistance in the upper soil increases (see De Kauwe et al., 2015, 2020b).

2.4.3 Dry soil approximation

Under extremely dry soil water conditions, the two-phase water retention curves used in JULES to calculate soil water potential (Brooks and Corey 1966; Genuchten 1980, all simulations in this study uses the Van Genuchten water retention curve) produces unrealistically low values of ψ_s. To address this, we implement a dry soil approximation following Webb (2000) and Schneider and Goss (2012), which model the log of the soil water potential as a linear function of the volumetric soil water content below a specific dry threshold;

$$\log(\psi_s) = \frac{\log(\psi_s^0) - log(\psi_s^*)}{S_l^*} S_l + \log(\psi_s^0) \tag{7}$$

where ψ_s is the soil water potential (MPa), ψ_s^0 is the soil water potential at zero volumetric soil water content (MPa), S_l^* and ψ_s^* are the soil water content (m^{3}m$^(-3)$) and soil water potential (MPa) bellow which the dry soil approximation applies. The values of S_l^* and ψ_s^* are chosen to satisfy the following conditions: one, the soil water potential is equal for both the dry soil approximation and the two-phase water retention curve at $S_l = S_l^*$; two, the gradient of the dry soil approximation is equal to the gradient of the two-phase water retention curve at $S_l = S_l^*$, e.g.;

$$\left.\frac{\mathrm{d}\log(\psi_s)}{\mathrm{d}S_l}\right|_{S_l = S_l^*, \psi_s = \psi_s^*} = \frac{\log(\psi_s^0) - log(\psi_s^*)}{S_l^*} \tag{8}$$

2.4.4 Xylem impairment models

Hydraulic conductance models in LSMs typically assume instantaneous recovery of conductance post drought stress. As a result, the xylem conductance function $k(\psi)$ does not change with time. However, any embolism that causes xylem impairment

https://doi.org/10.5194/egusphere-2026-4729
Preprint. Discussion started: 31 August 2026

could persist over a prolonged to indefinite period. Here, we implement two xylem impairment schemes in JULES to capture longer-term hydraulic damage.

The first impairment model, "k_{max}-impaired", is a modification of that described by Mackay et al. (2015). It assumes that impairment accumulates progressively as the drought develops, such that the magnitude of drought legacy effects depends on both drought intensity and duration. The k_{max}-impaired formulation also allows for partial recovery of hydraulic conductance following stress release.

The second impairment model, "Trunk-impaired", assumes hydraulic damage is determined by the most severe drought stress experiences, with legacy effects governed by the minimum conductance reached during the event. As with the Kmax-impaired, successive droughts can further reduce conductance if they generate more severe stress than previously experienced. However, unlike kmax-impaired, conductance cannot recover once impaired; instead, it is constrained by the historic minimum value it reached during the stress. Consequently, recovery can only occur through processes not represented in the current implementation, such as the production of new xylem tissue.

2.4.4.1 k_{max}-impaired

The model operates in a sequence: (i) first it determines an impaired maximum conductance, $k_{max}(t+\Delta t)$; and (ii) then it updates the scale and shape parameters of the hydraulic vulnerability curve (b and c). Mackay et al. (2015) calculated $k_{max}(t+\Delta t)$ as the unimpaired conductance at the predawn ψ_l each day. Here, instead of updating k_{max} to be equal to that of the unimpaired predawn k_{max}, we modify the Mackay et al. (2015) model to update k_{max} each time step based on the impaired k_{max} and the current conductance in both the leaves, k_l and roots, k_r. The aim of this modification is to capture the potential impact of daily water stress in the canopy due to high VPD as a canopy stressor, following the hypothesis that it may be a key contributor to embolism under specific hot and dry conditions (Schönbeck et al., 2022). To update the maximum conductance for the next time step, $k_{max}(t+\Delta t)$, we first calculate a stem conductance as the weighted average of the hydraulic conductance at the leaf and root water potentials:

$$k_{stem}(t) = w_l k_l(t) + (1 - w_l) k_r(t) \tag{9}$$

where w_l is the weighting of the leaf conductance, set to 0.4 to represent a balanced contribution of leaf and root hydraulic limitations under well-watered conditions.

To allow for gradual impairment, the maximum conductance is then calculated as the weighted average of $k_{stem}(t)$ and the current maximum conductance:

$$k_{max}(t+\Delta t) = w_{k_{stem}} k_{stem}(t) + (1 - w_{k_{stem}}) k_{max}(t) \tag{10}$$

https://doi.org/10.5194/egusphere-2026-4729
Preprint. Discussion started: 31 August 2026

Where $w_{k_{stem}}$ is the weight of the current conductance and $k_{max}(t)$ is the maximum conductance at the current time step. The value of $w_{k_{stem}}$, set to 0.01 for this study, controls the rate of impairment, with no impairment when $w_{k_{stem}} = 0$ and instantaneous impairment when $w_{k_{stem}} = 1$.

Updating the maximum conductance in this way leads to a small but continuous loss of conductance for trees under normal conditions. This behaviour reflects a simplification of the impairment process, whereby conductance loss accumulates progressively in response to hydraulic stress. In reality, embolism formation may be more strongly associated with exposure to severe drought thresholds than with continuous impairment across the full range of water potentials (Dietrich et al., 2019; Schuldt et al., 2020; Guan et al., 2022). Consequently, this formulation may overestimate low levels of conductance loss under non-drought conditions. This continuous loss of conductance is due to $k_l(t)$ and $k_r(t)$ only equalling $k_{max}(t)$ at night under well watered conditions and less than $k_{max}(t)$ otherwise. To prevent a continuous minor loss of conductance, a minimum conductance loss threshold is imposed (set to 6% of the unimpaired k_{max} for this work). The new maximum conductance bound by the minimum change threshold is given by the following equation;

$$k'_{\text{max}}(t+\Delta t) = \begin{cases} \frac{k_{\text{max}}(t)}{k_{\text{max}}(t)-\Delta k_{\text{max}}} k_{max}(t+\Delta t),\ k_{\text{max}}(t) - k_{max}(t+\Delta t) \geq \Delta k_{\text{max}} \\ k_{\text{max}}(t),\ k_{\text{max}}(t) - k_{max}(t+\Delta t) \leq \Delta k_{\text{max}} \end{cases} \tag{11}$$

Where Δk_{max} is the minimum conductance loss threshold. The inclusion of the fraction in the first case keeps the function continuous at the point where $k_{\text{max}}(t) - k_{max}(t+\Delta t) = \Delta k_{\text{max}}$

After calculating the new k_{max}, Mackay et al. (2015) recalculated the hydraulic vulnerability curve so that it retained the original shape at low levels of stress but reflected the reduced maximum conductance caused by impairment. Reproducing this procedure exactly requires repeatedly fitting a new vulnerability curve following each conductance update. To reduce computational cost, we instead used an approximation that preserves the overall shape of the impaired curve. Specifically, the parameters of the impaired vulnerability curve were chosen so that its midpoint and local slope matched those of the original vulnerability curve at an equivalent relative conductance (Fig. A1). This approach closely reproduces the behaviour of the original method while being computationally efficient. The equations used to calculate the impaired curve parameters are provided in appendix D.

Following sensitivity analysis of the parameters w_l, $w_{k_{stem}}$ and Δk_{max}, outlined in appendix G, we set their values to 0.5, 0.04 and 4% of the unimpaired k_{max}. This set of parameter values was chosen to induce a legacy change in PLC during 2022 but not during an average, non-drought, year.

2.4.4.2 Trunk-impaired

This model is built on two assumptions. One, xylem conductance does not recover post stress, it remains equal to that associated with the historic minimum water potential. Two, within a tree's water transport system, xylem impairment varies continuously with height, reflecting the smooth gradient between ψ_s and ψ_l (Fig 2). Since xylem impairment depends on the historical water

https://doi.org/10.5194/egusphere-2026-4729
Preprint. Discussion started: 31 August 2026

potential it follows that the impairment profile must also vary smoothly along the vertical axis. Here we propose an analytic model to implicitly account for variation in impairment along a tree's trunk without the need to explicitly segment the tree.

The first step is to define the impaired xylem conductance at some arbitrary height within the tree. We chose to model the impaired conductance, $k_{impaired}(h)$, as equal to the unimpaired conductance for the historic minimum water potential at that height, $k(\psi_{min}(h))$.

$$k_{impaired}(h) = k(\psi_{min}(h)) \tag{12}$$

Essentially, under water stress, xylem vessels are instantly and permanently damaged fixing their conductance at the current value. The xylem conductance remains at this impaired value until the tree experiences a greater level of water stress further reducing xylem conductance.

For a thin slice at some height h the flow of water through flow of water is given by Darcy's law;

$$E = \frac{k(\psi_{min}(h))}{\Delta h}\Delta\psi \tag{13}$$

where the through flow of water E is equal to the transpiration rate, Δh is the thickness of the slice, and $\Delta\psi$ is the change in water potential across the slice. Δh is thin enough for the conductance $k(\psi_{min}(h))$ to be constant within the slice. We can repeat the same equation, this time for the slice under the historic extreme (minimum) water potential,

$$E_{extreme} = \frac{k(\psi_{min}(h))}{\Delta h}\Delta\psi_{extreme} \tag{14}$$

where, $E_{extreme}$ is the historic transpiration rate and $\Delta\psi_{extreme}$ the historic change in water potential across the slice when the water potential was at its historic minimum. Since the conductance and width of the slice are equal in both equations, we can remove these by dividing the current transpiration rate by the historic transpiration rate.

$$\frac{E}{E_{historic}} = \frac{\Delta\psi}{\Delta\psi_{historic}} \tag{15}$$

This means the ratio of the change in water potential across the thin slice at the current and historic extreme conditions is constant with height. This ratio holds true for any slice along the trunk irrespective of size (see appendix E). Hence, by considering the difference in water potential across the whole trunk the current impaired transpiration rate is given by

$$E = \frac{\psi_l - \psi_s}{\psi_{lmin} - \psi_{rmin}}E_{historic} \tag{16}$$

where, ψ_l and ψ_s are the current leaf and root zone water potentials, and $\psi_{l\ min}$ and $\psi_{s\ min}$ are the historic minimum leaf and root zone water potentials. The historic transpiration rate can be calculated by integrating the unimpaired conductance curve from the historic minimum root to leaf ψ_l such that,

https://doi.org/10.5194/egusphere-2026-4729
Preprint. Discussion started: 31 August 2026

$$E = \frac{\psi_l - \psi_s}{\psi_{lmin} - \psi_{rmin}} \int_{\psi_{rmin}}^{\psi_{lmin}} k(\psi_{min}) d\psi_{min} \tag{17}$$

Tracking the level of xylem impairment within this model is done by updating the historic minimum leaf and root water potentials each time the current leaf or root water potential is less than the historic minimum. Changing the equation for the transpiration rate to equation 17 complicates the Newton Raphson estimation of the ψ_l from the transpiration rate. This complication arises from the fact that the value of the ψ_l may or may not be less than the historic minimum ψ_l. An updated version of the Newton Raphson method capable of accounting for this is given in the appendix F.

2.4.5 Impairment and the hydraulic cost function

The hydraulic cost function in the Profit-Max model (equation 3) depends directly on the plant hydraulic conductance. We choose to evaluate the hydraulic cost function using the unimpaired conductance curve for both the healthy and impaired cases, rather than the impaired conductance. This formulation assumes that stomatal regulation responds to leaf water content (proxied by ψ_l) as an integrated indicator of hydraulic stress, rather than directly sensing changes in hydraulic conductance. In this framework, hydraulic impairment influences stomatal behaviour indirectly through its effects on leaf water potential and the associated hydraulic risk. This is consistent with stomatal optimization theories, which assume that stomatal regulation responds to leaf water status rather than directly sensing xylem hydraulic conductance.

Although the impaired conductance curve is not explicitly used in the hydraulic cost function, hydraulic impairment still influences the optimisation indirectly through its effect on the ψ_l required to sustain a given flux. Consider two identical trees under the same environmental conditions, one healthy and the other hydraulically impaired. For a given stomatal conductance both trees exhibit identical carbon assimilation and transpiration rates, and thus identical carbon gain. However, because the impaired tree has lower hydraulic conductance , it must operate at a more negative ψ_l to sustain the same transpiration rate. This increases the hydraulic cost and reduces the profit relative to the healthy tree. As a result, hydraulic impairment shifts the Profit-Max solution towards lower stomatal conductance and less negative ψ_l. The models therefore predict that, following hydraulic impairment, trees reduce water usage to avoid further hydraulic stress, even at the expense of reducing carbon gain.

3 Model experiments

3.1 2022 summer drought

To assess the predictive capability of the CTRL, stomatal optimisation and legacy impairment model versions, we construct a three-year forcing ensemble consisting of the 2022 drought year preceded and followed by all possible combinations of the years 2011-2017. Including a non-drought year before 2022 also allows us to capture any background hydraulic impairment at the onset of the drought.

https://doi.org/10.5194/egusphere-2026-4729
Preprint. Discussion started: 31 August 2026

Model	GPP RMSE ($g\ C\ m^{-2}\ d^{-1}$)	GPP R^2	LE RMSE ($W\ m^{-2}$)	LE R^2
CTRL	4.15	0.23	47.7	0.03
Profit-Max	2.21	0.783	38.4	0.37

Table 1. Goodness of fit to flux tower observations for the CTRL and Profit-Max model GPP and LE predictions during the summer (June to September) for the average year (2011 to 2017). All data was averaged over a daily time scale, including night tine data, before calculating the respective goodness of fit measures

To estimate the predicted immediate and legacy impact of the 2022 drought on GPP and LE, we generate a corresponding non-drought forcing data set by replacing the 2022 drought year with a randomly selected year from 2011-2017. This process is repeated three times for each drought ensemble member. Impacts are then calculated as the difference between drought and non-drought simulations and averaged across all ensemble members.

3.2 Simulating more extreme drought scenarios

To explore modelled responses to future droughts more extreme than the 2022 drought, we constructed a three-year sequence of increasing drought intensity by repeating the 2022 forcing data, with precipitation in the second and third years reduced to one-half and one-quarter of the original 2022 totals respectively. To represent the dry spring conditions observed in 2025, all rainfall from March to May is removed from the second and third drought years. As with the previous experiment, an average year non-drought year is prepended to capture any background impairment.

We further extend the 2022 drought experiment by substituting the modified half- and quarter- precipitation years for the original 2022 forcing, allowing us to isolate the effects of increased drought severity on GPP and LE.

Initial conditions (e.g. soil water content) for each experiment were obtained by separately running the CTRL and Profit-Max models for the period 2011 to 2017. No xylem impairment model was applied during this 'spin-up' period, ensuring zero impairment at the start of each experiment.

4 Results

During the first half of the average year (i.e. the year prior to the drought), all models overestimate GPP and LE relative to observations (Fig 3), likely due to the satellite-derived LAI climatology imposing an earlier onset of growth than is evident in the GPP and LE fluxes.

During the summer months of the average year, the CTRL model shows a marked under estimation of GPP and LE relative to observations (Fig 3), reflecting an over-sensitivity to soil moisture stress. In contrast, both stomatal optimisation models show a much smaller under-prediction of GPP and LE during the summer months compared with observations (Table 1).

The inclusion of the impairment model did not significantly impact simulated GPP and LE under normal conditions prior to a drought. The unimpaired Profit-Max model predicted an average GPP and LE for the normal year prior to drought of

https://doi.org/10.5194/egusphere-2026-4729
Preprint. Discussion started: 31 August 2026

$2,130$g C m^{-2} d^{-1} and 37W m^{-2}, respectively, with the k_{max}-impaired and Trunk-impaired models predicting annual GPP of $2,130$ and $2,130$ g C m^{-2} year^{-1} and annual LE of 36 and 37 W m^{-2}, respectively.

4.1 Ecosystem flux response to the 2022 drought

The Profit-Max model better predicts LE during the 2022 drought compared to the CTRL model (Fig 3). Comparing the CTRL model's LE to observations for the whole drought year gives a RMSE and R^2 values of 28W m^{-2} and 0 respectively. In contrast, the Profit-Max model gives a RMSE and R^2 values of 22W m^{-2} and 0.4 respectively.

During the drought, both impairment models simulate a small increases GPP and LE compared to the unimpaired model. For the k_{max} and whole trunk impairment models the average difference in prediction to the unimpaired Profit-Max model was, 1.6 and 0.1 g C m^{-2} d^{-1} for GPP and 7 and 1 W m^{-2} for LE, respectively. These small differences in fluxes indicate that drought (and atmospheric) conditions, rather than the representation of hydraulic impairment, is the main contributor to the predicted GPP and LE. Hydraulic impairment acted primarily as a secondary modifier of these responses, resulting in only modest divergence among model formulations.

4.2 Soil water content during the 2022 drought

During the 2022 drought the Ctrl and profit-max models predict comparable dry downs to observations in the top layers (fig **??**). In the deeper soil layers both models under predict water content, implying unrealistically large amounts of water extraction at depth. Following the drought (and other periods with a lack of rain) both models predict an unrealistically fast recovery in volumetric soil water content, compared to observation.

4.3 Impact of 2022 drought on hydraulic impairment

While both impairment models showed a sustained loss of hydraulic conductivity following the average year, the trunk-impaired model maintained a percentage loss of conductance (PLC) of 8% while the k_{max}-impaired model partially recovers from a peak PLC of 9% to an end of year PLC of 1% (Fig 5). This difference reflects the contrasting recovery assumptions in the two formulations: the kmax-impaired model permits partial recovery of conductance following drought, whereas the trunk-impaired model does not.

During the 2022 drought, the predicted PLC peaked near the end of the drought period (Fig 5), when water stress was greatest. Peak PLC for the trunk-impaired model (9%) was slightly lower than the unimpaired model's peak PLC (10%). This reduction occurs because the loss of conductance in the average year decreases transpiration and water uptake from the soil leading to an increased water availability during the drought. In contrast, the peak PLC for the k_{max}-impaired model (40%) is larger than that of the unimpaired model (10%) despite reaching a less negative ψ_l because the impaired vulnerability curve has a reduced k_{max} (Fig 3).

https://doi.org/10.5194/egusphere-2026-4729
Preprint. Discussion started: 31 August 2026

During 2023, both impairment models simulate a sustained loss of conductivity. The k_{max}-impaired model shows a maximum PLC of 53% relative to the unimpaired models 9%, while the whole trunk impairment model maintains a constant PLC of 9% through the year (Fig 5).

4.4 Legacy of the 2022 drought

Of the two impairment models, the k_{max}-impaired model simulated an average legacy change in both GPP and LE of -250 g C m^{-2} year^{-1} and -3 W m^{-2} respectively, in 2023. The magnitude of this legacy impact however is dependent on the choice of weightings used in the impairment model (appendix G). Increasing $w_{k_{stem}}$ or w_l will increase the legacy impact of the drought while increasing Δk_{max} will decrease the legacy impact. By contrast, the whole trunk impairment model simulated no significant legacy change in fluxes.

4.5 Assessing ecosystem resilience under intensified 2022 drought conditions.

We generated more extreme drought scenarios than observed (by intensifying the 2022 drought conditions) with the aim to explore potential future drought resilience in European oaks by experimentally intensifying the 2022 drought (see methods).

In these scenarios, progressive rainfall reduction leads to increasing hydraulic stress, most clearly observed through rising PLC in the later stages of the drought scenarios (Fig 7). Peak PLC reaches 11%, 55% and 10% for the unimpaired, k_{max}-impaired and trunk-impaired models respectively under the half-rainfall scenario, increasing further to 13%, 61% and 13% respectively under the quarter-rainfall scenario. These differences indicate substantially greater vulnerability to drought-induced hydraulic failure in the k_{max}-impaired configuration.

This escalation in the hydraulic stress is not apparent during the early part of the simulation. Peak GPP and LE show only small reductions across drought scenarios for both the unimpaired and impaired models (Fig 8), with a mid-April maximum occurring prior to the onset of the 2022 drought period. Root zone water potential remains close to zero across all models at this time, indicating near-saturated soil conditions and the absence of water limitation. Consequently, early-season fluxes are largely insensitive to imposed rainfall reductions.

Consistent with earlier results, the impaired models exhibit more conservative water use strategies relative to the unimpaired model (Fig 9). This is reflected in their less negative water potentials under extreme drought, particularly in the quarter rainfall scenario, where stress in the unimpaired model becomes significantly severe that its GPP falls below that of the impaired configurations from August onwards. While this conservative hydraulic behaviour buffers against hydraulic failure under extreme drought, it incurs a trade-off under well-watered conditions post drought, where impairment models achieve lower GPP due to restricted water use capacity (Fig 9). Under the half rainfall scenario, the k_{max}-impaired model simulates a significant legacy reduction in GPP and LE of -21% and -14% respectively. This legacy reduction increases to -26% and -14% under the quarter rainfall scenario. In contrast, the trunk-impaired model simulates a consistent small reduction in GPP and LE, -1% and -2% respectively, under the half rainfall scenario. Similar reductions in GPP and LE are modelled under the quarter rainfall scenario, -1% and -2% respectively.

https://doi.org/10.5194/egusphere-2026-4729
Preprint. Discussion started: 31 August 2026

To test these results are driven by 2023's climatology we repeat the experiment replacing 2023 with an average year (Fig 9). The results show no significant difference in PLC when compared to 2023.

5 Discussion

To predict the immediate and legacy effects of drought, we implemented a stomatal optimisation model (Profit-Max; Sperry et al., 2017) into the JULES LSM, extending this scheme to account for long term hydraulic impairment of the plant water transport system. We evaluated these modelling approaches against observation from the UK summer drought of 2022 at an oak woodland flux tower site in south-east England.

Consistent with previous studies incorporating plant hydraulics and stomatal optimisation into LSMs (De Kauwe et al., 2020a; Kennedy et al., 2019; Sabot et al., 2020; Alléon et al., 2025), profit max improved predictions of LE both before and during the 2022 drought compared to the standard CTRL model (RMSE: 18 and 27 W m^{-2} respectively verses observed LE). Of the two legacy impairment formulations, only the k_{max}-impaired model simulated a significant legacy reduction in GPP (-250 gC $m^{-2} year^{-1}$) and LE (-1.5 W m^{-2}) with a post drought PLC of 32% compared to 9% for the whole trunk legacy impairment model.

To explore future resilience under more extreme drought conditions, we repeated the experiment with reduced rainfall during the 2022 drought period. When spring rainfall was removed (similar to conditions in 2025) and precipitation was halved for the remainder of 2022, the k_{max}-impaired model simulated substantial legacy effects, with reductions of -21% and -14% in GPP and LE respectivly in 2023 (Fig 9), driven by sustained increases in PLC to 55%. In contrast, the trunk-impaired model showed minimal legacy impacts (a 1% and 2% reduction in GPP and LE respectively), with a lower post-drought PLC (10%).

Under the imposed extreme drought scenario, substantial conductance losses were simulated despite the maintenance of positive hydraulic safety margins. This reflects the assumptions of the model parametrisation and impairment formulations, which permit conductance losses before hydraulic safety margins approach zero. Whether the magnitude of simulated PLC under these conditions is consistent with observed hydraulic responses remains uncertain and warrants further evaluation against empirical site measurements.

Overall, our results suggest that the simulated hydraulic impacts of the 2022 drought at Alice Holt were modest, with both impairment schemes remaining below critical hydraulic failure thresholds (88% PLC). However, the magnitude and persistence of these responses were sensitive to the choice of impairment formulation and drought severity. Under intensified drought conditions, the kmax-impaired formulation simulated substantially larger legacy effects and greater hydraulic dysfunction, highlighting the potential importance of hydraulic memory processes for ecosystem carbon and water fluxes. These results emphasise the value of explicitly representing hydraulic legacy processes in LSMs, while also underscoring the need for further evaluation of modelled hydraulic responses against site-level observations.

https://doi.org/10.5194/egusphere-2026-4729
Preprint. Discussion started: 31 August 2026

5.1 Drought impact on UK Oak forests

Overall, our simulations indicated diverging hydraulic impact from the 2022 drought (maximum PLC values of 40% and 9% for the k_{max}-impaired and trunk-impaired models respectively). As the UK faces an increasing likelihood of similar droughts, robust assessment of species vulnerability to extreme events is essential. Only the k_{max}-impaired model produced significant post-drought legacy effects, and these were relatively small, suggesting that the simulated ecosystem responses at Alice Holt were driven primarily by the direct effects of drought rather than persistent hydraulic impairment. However, these findings should be interpreted cautiously, as the hydraulic responses have not been evaluated against site-level measurements of plant water status, hydraulic function, or growth. Furthermore, oak species are comparatively drought tolerant (Urli et al., 2014), and broader cross-species analyses will be required to assess the generality of these results. Under a more extreme drought scenario, long-term PLC increased to 55% and 10% for the k_{max}-impaired and trunk-impaired models, respectively, indicating that projected responses are sensitive to both drought severity and assumptions regarding hydraulic impairment and recovery.

5.2 Comparison with existing drought legacy schemes

The two models of xylem impairment we tested make contrasting assumptions regarding the rate at which xylem impairment accumulates under stress. The whole trunk model assumes instantaneous impairment, whereas the k_{max}-impaired model simulates progressive impairment through time. The k_{max}-impaired model approaches an instantaneous impairment formulation as the conductance weighting parameter ($w_{k_{stem}}$ in equation 10) approaches one. However, under such parametrisations a constant water potential can repeatedly reduce conductance at successive timesteps, resulting in runaway impairment. The impairment threshold Δk_{max} (equation 11) was therefore introduced to prevent this behaviour. Alternatively, Mackay et al. (2015) avoided this issue by linking impairment to predawn water potential and the associated unimpaired conductance. The behaviour of the k_{max}-impaired formulation is sensitive to the choice of weights, highlighting the importance of better empirical constraints on hydraulic impairment dynamics and motivating the parameter sensitivity analysis (fig A2).

A limitation of our choice of a small impairment threshold (6%) is that it enables conductance losses even under relatively benign conditions, whereas empirical evidence suggests that embolism formation may be concentrated during periods of severe drought (Dietrich et al., 2019; Schuldt et al., 2020; Guan et al., 2022). Future model developments could explore threshold-based representations of embolism formation that better separate mild hydraulic stress from the onset of significant xylem dysfunction.

By using predawn water potential to determine k_{max}-impaired, Mackay et al. (2015) effectively assume that legacy xylem impairment is governed by the soil water potential. While predawn water potential may largely reflect prior hydraulic stress, it dampens the influence of extreme diurnal daytime ψ_l on hydraulic impairment, particularly towards the top of the tree. Consequently, this modelling approach may underestimate the impact of transient but severe diurnal declines in ψ_l.

In contrast, the models by Lu et al. (2020) and Yao et al. (2025) determine legacy impairment based on the ψ_l. While ψ_l partially depends on the soil water potential it most closely reflects the transient impact of VPD on water stress towards the top of the tree. Consequently, this modelling approach may overestimate the impact of transient but severe diurnal declines in ψ_l.

https://doi.org/10.5194/egusphere-2026-4729
Preprint. Discussion started: 31 August 2026

Our k_{max}-impaired model is designed to capture the impact on legacy impairment of both the leaf and soil water potentials with a weighted average of the leaf and root conductance (equation 9) to calculate impairment. Though this allows for differing impacts of the leaf and root conductance's on legacy impairment it introduces an additional fit parameter not directly related to a tree's physical traits.

Ruffault et al. (2022) and Paschalis et al. (2024) partition the hydraulic model by tree organ to capture the impact of differing organ conductance and hydraulic impairment. Such partitioning enables testing of the 'hydraulic segmentation' hypothesis which posits that: plants protect the stem by increasing hydraulic resistance and vulnerability in expendable organs such as leaves (Zhao et al., 2026). Subsequently by not segmenting by organ our impairment models may overestimate the legacy impact on the trunk.

The models by Ruffault et al. (2022) and Paschalis et al. (2024) approximate conductance within each organ as constant (done to enable the modelling of hydraulic capacitance). This approximation falters when the difference in water potential across the organ is large, as is common within the trunk. This can be solved by sub-partitioning the trunk enabling conductance, and hence hydraulic impairment, to change, moving up the trunk. The whole trunk impairment model implicitly tracks hydraulic impairment as a function of height avoiding the need to segment the trunk. This enables the model to capture how the relative impacts of ψ_s and ψ_l on hydraulic impairment changes moving up the tree. The model does however assume that the extreme leaf and soil water potentials occur at the same time. It is also not clear how to mathematically include hydraulic capacitance in this model without segmentation, as in the models by Ruffault et al. (2022) and Paschalis et al. (2024).

Our results showed that despite impairment of xylem function (PLC of 40% and 9% at the end of 2022 for k_{max} and whole trunk impairment respectively), only the k_{max}-impaired model predicted a significant legacy effect on GPP and LE fluxes (Fig 6). This is consistent with the limited legacy effects predicted by Sabot et al. (2022b) where, despite significant canopy PLC, simulated hydraulic legacy effects were small and short-lived (2 months). In contrast, the legacy impairment model proposed by Paschalis et al. (2024) predicted a systematic reduction in GPP post drought and all three legacy models described by Yao et al. (2025) predict systematic reductions in fluxes following the drought period. The simplest explanation for the apparent discrepancy, is that the 2022 drought we examined was less extreme than the summer events simulated by those studies. Notably, while our study found consistency between the impairment model predictions and the LE fluxes, Paschalis et al. (2024) found that the observed GPP was better simulated by their non-legacy model. Yao et al. (2025) found a more mixed picture, for the 40 days immediately following the drought, transpiration was best simulated by non-legacy models while GPP was better predicted by two of their three legacy impairment models. Notably the magnitude of drought legacy is sensitive not only to the drought itself but the impacted species and weather conditions following the drought (Jiao et al., 2021). Studies on drought legacy impact on GPP fluxes have found a mix of positive, negative and no significant legacy effects (Yao et al., 2025). These studies, alongside ours, highlight the complexity of evaluating approaches designed to capture drought legacy effects when analysis is limited to ecosystem-scale fluxes alone. Resolving drought legacy effects therefore requires concurrent measurements of plant water status, hydraulic function (including embolism or loss of conductivity), and structural turnover. This gap may be partially addressed using optical cavitation imaging approaches (Brodribb et al., 2016, 2017) , applied to leaf petioles or minor veins, which can provide high-resolution, time-resolved observations of embolism formation and spread.

https://doi.org/10.5194/egusphere-2026-4729
Preprint. Discussion started: 31 August 2026

5.2.1 Choice of hydraulic cost function

When incorporating xylem impairment into the stomatal optimisation framework we chose to calculate the hydraulic cost function (equation 3) using the unimpaired vulnerability curve. Preliminary testing indicated that this modelling decision substantially alters post-drought stomatal behaviour. Specifically, updating the hydraulic cost function to reflect the impaired vulnerability curve causes trees to tolerate greater hydraulic risk and maintain higher stomatal conductance following drought. In contrast, calculating the hydraulic cost function from the unimpaired vulnerability curve promotes more conservative stomatal regulation and lower hydraulic risk. Consequently, the magnitude of simulated drought legacy effects is sensitive not only to the representation of hydraulic impairment itself, but also to how impairment is coupled to stomatal regulation. Further work is required to determine which assumption is most consistent with observed post-drought stomatal behaviour.

By adopting the unimpaired vulnerability curve in the cost function, we implicitly assume that the stomata respond solely to leaf water content (proxied by ψ_l in stomatal optimisation models) and are not directly sensitive to the degree of hydraulic impairment elsewhere in the hydraulic pathway. Under this interpretation, cumulative xylem damage influences stomatal regulation indirectly through its effects on water transport and leaf water content, rather than through an explicit impairment signal. This assumption is consistent with the view that stomata respond primarily to local hydraulic status rather than directly to whole-plant hydraulic dysfunction.

5.2.2 Mechanisms of xylem recovery

Our tested modeling approach focuses on defining legacy in the year post a specific event. In the long-term, the incorporation of xylem impairment into LSMs is done with the goal of producing more robust, operational forecasts of drought impacts, as one summer extreme blends into the next due to a changing climate. To achieve this aim, any approach will need to be extended to predict long-term xylem recovery. Recovery of hydraulic conductance following embolism has been hypothesised to occur through either embolism refilling (Klein et al., 2018) or the production of new conductive tissue through xylem growth (Brodribb et al., 2010; Trugman et al., 2018). However, the prevalence of embolism refilling under field conditions remains debated, and recent work has argued that long-term recovery of hydraulic function is more commonly achieved through xylem replacement rather than repair of embolised conduits (Deans et al., 2026). Mackay et al. (2015) represent recovery through a refilling-like process by resetting the impaired vulnerability curve according to the unimpaired conductance associated with the predawn water potential each day. As discussed by Mackay et al. (2015) a better approach than refilling at a given time each day would be to model refilling when a set of appropriate conditions are met, for example applying refilling when water potential exceeds a given threshold. In addition to when refilling occurs any model would also need to consider the rate at which xylem refill.

Over a longer timescale, the continued growth of new xylem by a tree will restore (and potentially increase) its hydraulic conductivity. In dynamic vegetation models that explicitly simulate stem wood growth and partitioning between sapwood and hard wood, impairment schemes could be readily incorporated. However, this is not typically the case in many LSMs, including JULES. Paschalis et al. (2024) model how the growth of xylem impact hydraulic recovery by separately tracking the level of

https://doi.org/10.5194/egusphere-2026-4729
Preprint. Discussion started: 31 August 2026

impairment of groups of xylem grown at different times (xylem grown before a drought will be more impaired than those grown after). The conductivity of the tree is calculated by treating the different age groups of xylem in parallel. This segmentation of xylem by date of growth is better able to capture the nuanced impact of differing historic drought exposure and changes in xylem growth rate compared to simply (partially) restoring the impaired vulnerability curve. The model could also be extended to include the influence of changes in xylem structure (Oberleitner et al., 2022, e.g. reduced diameter) on conductance and hydraulic vulnerability in response to drought stress.

Partial hydraulic recovery immediately following reduced hydraulic stress is present in several impairment models (Mackay et al., 2015; Lu et al., 2020; Yao et al., 2025), including our k_{max}-impaired model. These approaches arguably lack theory (or a solid data underpinning) about how and to what extent recovery is achievable Insight into potential mechanisms for instantaneous partial recovery of hydraulic conductance post drought is necessary to build more realistic hydraulic legacy models.

5.3 Future directions

While this work has sought to improve how the JULES LSM simulates stomatal dynamics and legacy damage to hydraulic transportation, trees have evolved additional strategies to avoid hydraulic failure under drought stress. For example, a tree's internal water storage (capacitance) helps maintain stable internal water potentials, buffering stomatal response to atmospheric moisture stress, and potentially delaying the onset of hydraulic impairment. Currently, JULES does not represent this process, highlighting an important avenue for model improvement.

During drought, some trees shed their leaves to reduce water loss and lower hydraulic vulnerability. Using a stomatal optimisation model, Sabot et al. (2022b) showed that leaf shedding, suppressed foliage growth or a reducing crown size over time, can act as a strategy to mitigate drought risk in a Eucalyptus woodland in Australia. LSMs, including JULES, incorporate parametrisation to capture drought-induced deciduousness (not enabled in this study); however, the thresholds triggering this process lack a strong theoretical or empirical support, sometimes resulting in unrealistic behaviour (De Kauwe et al., 2017).

6 Conclusion

We introduced a stomatal optimisation scheme and two representations of drought-induced hydraulic impairment into the JULES LSM and assessed their effects on ecosystem carbon and water fluxes following the 2022 UK summer drought and under more severe future drought scenarios. The stomatal optimisation scheme improved simulations of GPP and LE relative to the standard JULES configuration (RMSE values for predicted GPP improved from 4.15 to 2.21 $gC\ m^{-2}\ d^{-1}$ during the summer, table 1), while the hydraulic impairment schemes enabled the representation of drought legacy effects arising from persistent reductions in xylem conductance. Although both hydraulic schemes predicted sustained losses of hydraulic conductance following drought (reaching $9-32\%$ following the 2022 drought and $13-56\%$ under the extreme drought scenario), the resulting legacy effects on GPP and LE were generally modest. The magnitude and persistence of these effects depended on assumptions regarding hydraulic impairment and recovery, highlighting a key source of uncertainty in projections of for-

https://doi.org/10.5194/egusphere-2026-4729
Preprint. Discussion started: 31 August 2026

est drought responses. Under more severe drought scenarios, hydraulic dysfunction increased substantially and differences between impairment formulations became more pronounced, but effects on ecosystem carbon uptake and evapotranspiration remained comparatively limited. Overall, our results suggest that the 2022 drought caused only modest long-term impacts on carbon and water fluxes at the Alice Holt oak forest, while demonstrating the feasibility of representing hydraulic legacy processes within a LSM. More broadly, our findings highlight the difficulty of evaluating hydraulic legacy schemes using ecosystem flux measurements alone. Robust assessment of modelled hydraulic impairment and recovery will require complementary observations of plant water status, hydraulic conductivity, embolism occurrence, and growth across the soil-plant-atmosphere continuum.

Code availability. The model source code can be accessed freely after registration at https://jules-lsm.github.io/access_req/JULES_access.html. In this paper we used the JULES branch found at: https://code.metoffice.gov.uk/svn/jules/main/branches/dev/jakebaguley/Xylem_imparement. All analysis code is freely available from: https://github.com/CaleBaguley/UK-Ham_stom_opt_work.

Appendix A Leaf area index phenology construction

The spacial and temporal resolutions of the MODIS data set are $500m$ by $500m$ and four days respectively. We first select those LAI observations flagged within the MODIS catalogue as good quality and without significant cloud cover. We calculate the daily average LAI of pixels within 500m of the Alice Holt site (51°10'34.8"N 0°50'25.5"W). The full time series is converted to a daily phenology by averaging LAI for each day of the year, across all years. Any days without observations at this stage are filled using liner interpolation. Finally, a 100-day moving average is applied to smooth the phenology with the smoothing window wrapping around the start and end of the year to avoid a discontinuity.

Appendix B Vulnerability curve parameter calculation from P50 and P88

For the cumulative Weibull distribution used by the Profit max model, the shape and scale parameters, c and b respectivly, can be calculated as follows:

$$c = \frac{\ln\left(\frac{\ln(0.5)}{ln(0.12)}\right)}{\ln\left(\frac{P_{50}}{P_{88}}\right)} = \frac{-1.118}{\ln\left(\frac{P_{50}}{P_{88}}\right)} \tag{B1}$$

$$b = \frac{P_{50}}{(-\ln(0.5))^{1/c}} = \frac{P_{88}}{(-\ln(0.12))^{1/c}} \tag{B2}$$

For the hydraulic vulnerability curve used by the SOX model, the scale parameter b is equal to the P_{50} and the shape parameter c can be calculated as follows:

https://doi.org/10.5194/egusphere-2026-4729
Preprint. Discussion started: 31 August 2026

$$c = \frac{\ln\left(\frac{1}{0.12} - 1\right)}{\ln\left(P_{88}\right) - \ln\left(P_{50}\right)} = \frac{1.992}{\ln\left(P_{88}\right) - \ln\left(P_{50}\right)} \tag{B3}$$

Appendix C Newton Rapshon method for estimating leaf water potential from transpiration

For both hydraulic vulnerability curves there is no analytic solution for calculating the leaf water potential ψ_l from the transpiration rate E and root zone water potential ψ_r. Instead, we approximate ψ_l using a Newton-Raphson method. In the case of the leaf water potential, ψ_l, the update step for the Newton Raphson method takes the form;

$$\psi_{l\ n+1} = \psi_{l\ n} - \frac{E(\psi_{l\ n}) - E_{target}}{\frac{dE}{d\psi_l}|_{\psi_l = \psi_{l\ n}}} \tag{C1}$$

where E_{target} id the transpiration rate calculated from the stomatal conductance and vapour pressure deficit, $E(\psi_{l\ n})$ is given by intergrating over the vulnerability curve;

$$E(\psi_l) = \int_{\psi_r}^{\psi_l} k(\psi) d\psi \tag{C2}$$

and $\frac{dE}{d\psi_l}$ is given by the hydraulic conductance at the current leaf water potential, $k(\psi_{l\ n})$.

For the cumulative weibull distribution, used by the Profit max model, the integral over the vulnerability curve takes the form;

$$E(\psi_l) = k_{max}\left[\gamma\left(\frac{1}{c}, \left(\frac{\psi}{b}\right)^c\right)\right]_{\psi=\psi_r}^{\psi=\psi_l} \tag{C3}$$

where γ is the lower incomplete gamma function.

For the hydraulic vulnerability curve used by the SOX model, the integral over the vulnerability curve takes the form;

$$E(\psi_l) = k_{max}\left[\psi\ {}_2F_1\left(1, \frac{1}{c}; 1 + \frac{1}{c}; -\left(\frac{\psi}{b}\right)^c\right)\right]_{\psi=\psi_r}^{\psi=\psi_l} \tag{C4}$$

where ${}_2F_1$ is the Gaussian Hypergeometric series.

We note that for both hydraulic vulnerability curves, the initial guess for the leaf water potential is set to the root zone water potential. We chose to iterate a total of three times, as opposed to iterating until some convergence criteria, as this was found to be sufficiently accurate for our purposes and reduces computational cost of repeatedly checking convergence for all 1000 sample points per pft and tile.

https://doi.org/10.5194/egusphere-2026-4729
Preprint. Discussion started: 31 August 2026

Appendix D k_{max}-impaired updated scale and shape parameters

The equations for calculating the scale and shape parameters from the new impaired $k + max$ and unimpaired vulnerability curve for the cumulative Weibull distribution are listed below.

The new scale parameter, b', is given by,

$$b' = b\left(1 - \ln\frac{k'_{max}}{k_{max}}\right)^{\frac{1}{c}} \tag{D1}$$

where, b is the original scale parameter, k'_{max} and k_{max} are the new impaired and unimpaired maximum conductance respectively and c is the original shape parameter.

The new shape parameter, c', is given by,

$$c' = c\left(\frac{b'}{c'}\right)^{c} \tag{D2}$$

Appendix E Extending from a thin slice to the full trunk for the whole trunk impairment model.

As described in the main text, the ratio of the imparied transpiration that under the historic extreme leaf and root water potentials is equal to the ratio of the current change in water potential to the historic change in water potential for a thin slice of the trunk at any height.

$$\frac{E}{E_{historic}} = \frac{\Delta\psi(h)}{\Delta\psi_{historic}(h)} \tag{E1}$$

where the height dependence of the change in water potential has been made explicit. To extend this from a thin slice consider two thin slices at different heights, h_1 and h_2. We can write the ratio of the combined current difference in water potential at both heights to the combined historic difference in water potential at both heights as follows;

$$\frac{\Delta\psi(h_1) + \Delta\psi(h_2)}{\Delta\psi_{historic}(h_1) + \Delta\psi_{historic}(h_2)} \tag{E2}$$

Using the height independence of the ratio of the current change in water potential to the historic change in water potential for a thin slice, we can rewrite this as follows;

$$\frac{\Delta\psi(h_1) + \Delta\psi(h_2)}{\Delta\psi_{historic}(h_1) + \Delta\psi_{historic}(h_2)} = \frac{\Delta\psi(h_1) + \Delta\psi(h_1)\frac{\Delta\psi_{historic}(h_2)}{\Delta\psi_{historic}(h_1)}}{\Delta\psi_{historic}(h_1) + \Delta\psi_{historic}(h_1)\frac{\Delta\psi(h_2)}{\Delta\psi(h_1)}} \tag{E3}$$

Rearranging this equation gives the following;

https://doi.org/10.5194/egusphere-2026-4729
Preprint. Discussion started: 31 August 2026

$$\left(\frac{\Delta\psi(h_1)+\Delta\psi(h_2)}{\Delta\psi_{historic}(h_1)+\Delta\psi_{historic}(h_2)}\right)^2=\left(\frac{\Delta\psi(h_1)}{\Delta\psi_{historic}(h_1)}\right)^2 \tag{E4}$$

Taking the square root of both sides we can see that the ratio of the combined current change in water potential to the combined historic change in water potential for two thin slices is equal to the ratio of the current change in water potential to the historic change in water potential for a single thin slice;

$$\frac{\Delta\psi(h_1)+\Delta\psi(h_2)}{\Delta\psi_{historic}(h_1)+\Delta\psi_{historic}(h_2)}=\frac{\Delta\psi(h_1)}{\Delta\psi_{historic}(h_1)}=\frac{\Delta\psi(h_2)}{\Delta\psi_{historic}(h_2)} \tag{E5}$$

Given this works for two thin slices we can extend this to any number of thin slices, including the full trunk such that;

$$\frac{E}{E_{historic}}=\frac{\psi_l-\psi_r}{\psi_{l\ historic}-\psi_{r\ historic}} \tag{E6}$$

By rearranging this equation we get the equation for the current impaired transpiration, E, in the main text.

Appendix F Whole trunk impairment update to Newton Raphson method.

When solving for the leaf water potential first we check if the new rootzone water potential is less than the historic rootzone water potental, we update the historic rootzone water potential to the current rootzone water potential. For the leaf water potential there are two possible situations, ether the current leaf water potnetial is less negative than the historic leaf water potential, or the current leaf water potential is grater than the historic leaf water potential. Since we don't know which of these situations is correct a priori, we need to solve both cases and then check which is correct.

For the first case when the current leaf water potential is grater than the historic leaf water potential, its value is simply given by;

$$\psi_l=\psi_r+\frac{E_{target}}{E_{historic}}(\psi_{l\ historic}-\psi_{r\ historic}) \tag{F1}$$

where E_{target} is the transpiration rate calculated from the stomatal conductance and vapour pressure deficit, and $E_{historic}$ is the transpiration rate calculated under the historic extreme leaf and root water potentials.

$$E_{historic}=\int_{\psi_{r\ historic}}^{\psi_{l\ historic}}k(\psi)d\psi \tag{F2}$$

If the value for ψ_l calculated in this way is grater than the historic minimum leaf water potential $\psi_{l\ historic}$ then this is the correct solution, otherwise we need to use the Newton Raphson method to solve for ψ_l as described in appendix C, but with the following change to the transpiration equation;

https://doi.org/10.5194/egusphere-2026-4729
Preprint. Discussion started: 31 August 2026

$$E(\psi_l) = \frac{\psi_l - \psi_r}{\psi_l - \psi_{r\ historic}} \int_{\psi_{r\ historic}}^{\psi_l} k(\psi) d\psi \tag{F3}$$

Where the historic leaf water potential has been replaced by the current leaf water potential as it is the new extreme.

Appendix G k_{max} impairment model parameter sensitivity investigation

To test the sensitivity of the k_{max} impairment model to the parameters w_l, $w_{k_{stem}}$ and Δk_{max} we ran a series of 2022 simulations, systematically varying the three parameters. The parameters w_l, $w_{k_{stem}}$ and Δk_{max} were varied over the ranges 0 to 1, 0 to 0.1, and 0 to 0.1 respectively. We limit $w_{k_{stem}}$ to the range 0 to 0.1 to avoid significant conductance loss under normal (non-drought) conditions and Δk_{max} to the range 0 to 0.1 as beyond 0.1 it prevents any legacy PLC during 2022. For each combination of the three model parameters we simulated a single 2022 drought year, recording the maximum PLC reached during the year and the PLC at the end of 2022. To investigate the sensitivity of each individual parameter we calculate the median of the maximum simulated PLC in 2022, and the simulated PLC post 2022, averaging across the two non-varying parameters (figure A2).

Results of our sensitivity analysis show, increasing w_l leads to an increased PLC due to the conductance in the leaf being less than that of the roots resulting in a more negative k_{stem}. Increasing $w_{k_{stem}}$ leads to no apparent increase in PLC over the small range simulated, beyond this range we expect increasing $w_{k_{stem}}$ to increase the maximum PLC reached (the higher $w_{k_{stem}}$ the faster impairment occurs). When $w_{k_{stem}}$ is set to zero no impairment occurs irrespective of the other parameters. Finally, increasing Δk_{max} leads to a reduction in simulated PLC the system being insufficiently stressed for the loss of conductance to exceed larger thresholds.

Excluding simulations where $w_{k_{stem}} = 0$ we find a median Maximum PLC reached of 10% and median post 2022 PLC of 0.7%. Both occurred when $w_l = 0.5$, $w_{k_{stem}} = 0.04$, and $\Delta k_{max} = 0.04 k_{max}$.

Author contributions. JCB and MGDK designed the research in consultation with TQ, LR, and PM. JCB and MGDK developed and implemented the model. JCB carried out all the analysis and wrote the original manuscript draft. MCB processed the eddy-covariance data for the Alice Holt site. All authors contributed to reviewing and editing the final manuscript.

Competing interests. No competing interests to be declared.

Acknowledgements. JCB, MGDK, TQ, LR, and PM acknowledges funding from the UK Natural Environment Research Council (NE/W010003/1). MCB acknowledges funding, for the work by Forest Research at the Alice Holt Flux Station, from a core programme responding to the Sci-

https://doi.org/10.5194/egusphere-2026-4729
Preprint. Discussion started: 31 August 2026

ence and Innovation Strategy for Forestry in Great Britain (2021–2026) to which Defra, Forestry Commission, and the Scottish and Welsh governments contribute. All data analysis and plots were generated using the Python language and the Matplotlib library.

https://doi.org/10.5194/egusphere-2026-4729
Preprint. Discussion started: 31 August 2026

References

Adams, H., Zeppel, M., Anderegg, W., Hartmann, H., Landhäusser, S., Tissue, D., Huxman, T., Hudson, P., Franz, T., Allen, C., Anderegg, L., Barron-Gafford, G., Beerling, D., Breshears, D., Brodribb, T., Bugmann, H., Cobb, R., Collins, A., Dickman, L. T., and McDowell, N.: A multi-species synthesis of physiological mechanisms in drought-induced tree mortality, 2017.

Alléon, J., Vuichard, N., Ottlé, C., Tuzet, A., Luyssaert, S., Cuntz, M., Limousin, J.-M., Kempf, J., and Peylin, P.: Plant Hydraulic Architecture for a Mechanistic Representation of Soil-Plant-Atmosphere Water Transfer in the Land Surface Model ORCHIDEE (r9107), Journal of Advances in Modeling Earth Systems, 17, e2024MS004 869, https://doi.org/https://doi.org/10.1029/2024MS004869, e2024MS004869 2024MS004869, 2025.

Anderegg, W. R. L., Berry, J. A., Smith, D. D., Sperry, J. S., Anderegg, L. D. L., and Field, C. B.: The roles of hydraulic and carbon stress in a widespread climate-induced forest die-off, Proceedings of the National Academy of Sciences, 109, 233–237, https://doi.org/10.1073/pnas.1107891109, 2012.

Anderegg, W. R. L., Hicke, J. A., Fisher, R. A., Allen, C. D., Aukema, J., Bentz, B., Hood, S., Lichstein, J. W., Macalady, A. K., McDowell, N., Pan, Y., Raffa, K., Sala, A., Shaw, J. D., Stephenson, N. L., Tague, C., and Zeppel, M.: Tree mortality from drought, insects, and their interactions in a changing climate, New Phytologist, 208, 674–683, https://doi.org/https://doi.org/10.1111/nph.13477, 2015.

Anderegg, W. R. L., Klein, T., Bartlett, M., Sack, L., Pellegrini, A. F. A., Choat, B., and Jansen, S.: Meta-analysis reveals that hydraulic traits explain cross-species patterns of drought-induced tree mortality across the globe, Proceedings of the National Academy of Sciences, 113, 5024–5029, https://doi.org/10.1073/pnas.1525678113, 2016.

Anderegg, W. R. L., Trugman, A. T., Badgley, G., Anderson, C. M., Bartuska, A., Ciais, P., Cullenward, D., Field, C. B., Freeman, J., Goetz, S. J., Hicke, J. A., Huntzinger, D., Jackson, R. B., Nickerson, J., Pacala, S., and Randerson, J. T.: Climate-driven risks to the climate mitigation potential of forests, Science, 368, eaaz7005, https://doi.org/10.1126/science.aaz7005, 2020.

Argles, A., Moore, J., Huntingford, C., Wiltshire, A., Harper, A., Jones, C., and Cox, P.: Robust Ecosystem Demography (RED version 1.0): a parsimonious approach to modelling vegetation dynamics in Earth system models, Geoscientific Model Development, 13, 4067–4089, https://doi.org/10.5194/gmd-13-4067-2020, 2020.

Baldocchi, D., Falge, E., Gu, L., Olson, R., Hollinger, D., Running, S., Anthoni, P., Davis, K., Evans, R., Fuentes, J., Goldstein, A., Katul, G., Law, B., Lee, X., Malhi, Y., Meyers, T., Munger, J., Oechel, W., and Wofsy, S.: FLUXNET: A New Tool to Study the Temporal and Spatial Variability of Ecosystem-Scale Carbon Dioxide, Water Vapor, and Energy Flux Densities, Bulletin of the American Meteorological Society, 82, 2415–2434, https://doi.org/10.1175/1520-0477(2001)082<2415:FANTTS>2.3.CO;2, 2001.

Bastos, A., Ciais, P., Friedlingstein, P., Sitch, S., Pongratz, J., Fan, L., Wigneron, J.-P., Fu, Z., Anthoni, P., Arneth, A., Haverd, V., Jain, A., Joetzjer, E., Knauer, J., Lienert, S., Loughran, T., Mcguire, P., Tian, H., Viovy, N., and Zaehle, S.: Direct and seasonal legacy effects of the 2018 heat wave and drought on European ecosystem productivity, Science Advances , 6, 1–14, https://doi.org/10.1126/sciadv.aba2724, 2020.

Best, M., Pryor, M., Clark, D., Rooney, G., Essery, R., Menard, C., Edwards, J., Hendry, M., Porson, A., and Gedney, N.: The Joint UK Land Environment Simulator (JULES), model description – Part 1: Energy and water fluxes, Geoscientific Model Development, 4, 677–699, https://doi.org/10.5194/gmd-4-677-2011, 2011.

Bonan, G., Williams, M., Fisher, R., and Oleson, K.: Modeling stomatal conductance in the Earth system: Linking leaf water-use efficiency and water transport along the soil-plant-atmosphere continuum, Geoscientific Model Development, 7, 2193–2222, https://doi.org/10.5194/gmd-7-2193-2014, 2014.

https://doi.org/10.5194/egusphere-2026-4729
Preprint. Discussion started: 31 August 2026

Brodribb, T., Bowman, D., Nichols, S., Delzon, S., and Burlett, R.: Xylem function and growth rate interact to determine recovery rates after exposure to extreme water deficit, The New phytologist, 188, 533–42, https://doi.org/10.1111/j.1469-8137.2010.03393.x, 2010.

Brodribb, T. J. and Cochard, H.: Hydraulic Failure Defines the Recovery and Point of Death in Water-Stressed Conifers, Plant Physiology, 149, 575–584, https://doi.org/10.1104/pp.108.129783, 2008.

Brodribb, T. J., Skelton, R. P., McAdam, S. A. M., Bienaimé, D., Lucani, C. J., and Marmottant, P.: Visual quantification of embolism reveals leaf vulnerability to hydraulic failure, New Phytologist, 209, 1403–1409, https://doi.org/https://doi.org/10.1111/nph.13846, 2016.

Brodribb, T. J., Carriqui, M., Delzon, S., and Lucani, C.: Optical Measurement of Stem Xylem Vulnerability , Plant Physiology, 174, 2054–2061, https://doi.org/10.1104/pp.17.00552, 2017.

Ciais, P., Reichstein, M., Viovy, N., Granier, A., Ogée, J., Allard, V., Aubinet, M., Buchmann, N., Carrara, A., Chevallier, F., Denoblet, N., Friend, A., Friedlingstein, P., Grünwald, T., Heinesch, B., Keronen, P., Knohl, A., Krinner, G., and Valentini, R.: Europe-wide reduction in primary productivity caused by the heat and drought in 2003, Nature, v.437, 529-533 (2005), 437, 2005.

Clark, D. B., Mercado, L. M., Sitch, S., Jones, C. D., Gedney, N., Best, M. J., Pryor, M., Rooney, G. G., Essery, R. L. H., Blyth, E., Boucher, O., Harding, R. J., Huntingford, C., and Cox, P. M.: The Joint UK Land Environment Simulator (JULES), model description – Part 2: Carbon fluxes and vegetation dynamics, Geoscientific Model Development, 4, 701–722, https://doi.org/10.5194/gmd-4-701-2011, 2011.

Cooper, H. M., Bennett, E., Blake, J., Blyth, E., Boorman, D., Cooper, E., Evans, J., Fry, M., Jenkins, A., Morrison, R., Rylett, D., Stanley, S., Szczykulska, M., Trill, E., Antoniou, V., Askquith-Ellis, A., Ball, L., Brooks, M., Clarke, M. A., Cowan, N., Cumming, A., Farrand, P., Hitt, O., Lord, W., Scarlett, P., Swain, O., Thornton, J., Warwick, A., and Winterbourn, B.: COSMOS-UK: national soil moisture and hydrometeorology data for environmental science research, Earth System Science Data, 13, 1737–1757, https://doi.org/10.5194/essd-13-1737-2021, 2021.

Cox, P.: Description of the TRIFFID dynamic global vegetation model, Hadley Centre Technical Note, 24, 2001.

De Kauwe, M., Kala, J., Lin, Y.-S., Pitman, A., Medlyn, B., Duursma, R., Abramowitz, G., Wang, Y., and Miralles, D.: A test of an optimal stomatal conductance scheme within the CABLE Land Surface Model, Geoscientific Model Development, 8, 431–452, https://doi.org/10.5194/gmd-8-431-2015, 2015.

De Kauwe, M. G., Medlyn, B. E., Walker, A. P., Zaehle, S., Asao, S., Guenet, B., Harper, A. B., Hickler, T., Jain, A. K., Luo, Y., Lu, X., Luus, K., Parton, W. J., Shu, S., Wang, Y.-P., Werner, C., Xia, J., Pendall, E., Morgan, J. A., Ryan, E. M., Carrillo, Y., Dijkstra, F. A., Zelikova, T. J., and Norby, R. J.: Challenging terrestrial biosphere models with data from the long-term multifactor Prairie Heating and CO2 Enrichment experiment, Global Change Biology, 23, 3623–3645, https://doi.org/https://doi.org/10.1111/gcb.13643, 2017.

De Kauwe, M. G., Medlyn, B. E., Ukkola, A. M., Mu, M., Sabot, M. E. B., Pitman, A. J., Meir, P., Cernusak, L. A., Rifai, S. W., Choat, B., Tissue, D. T., Blackman, C. J., Li, X., Roderick, M., and Briggs, P. R.: Identifying areas at risk of drought-induced tree mortality across South-Eastern Australia, Global Change Biology, 26, 5716–5733, https://doi.org/https://doi.org/10.1111/gcb.15215, 2020a.

De Kauwe, M. G., Medlyn, B. E., Ukkola, A. M., Mu, M., Sabot, M. E. B., Pitman, A. J., Meir, P., Cernusak, L. A., Rifai, S. W., Choat, B., Tissue, D. T., Blackman, C. J., Li, X., Roderick, M., and Briggs, P. R.: Identifying areas at risk of drought-induced tree mortality across South-Eastern Australia, Global Change Biology, 26, 5716–5733, https://doi.org/https://doi.org/10.1111/gcb.15215, 2020b.

De Kauwe, M. G., Sabot, M. E. B., Medlyn, B. E., Pitman, A. J., Meir, P., Cernusak, L. A., Gallagher, R. V., Ukkola, A. M., Rifai, S. W., and Choat, B.: Towards species-level forecasts of drought-induced tree mortality risk, New Phytologist, 235, 94–110, https://doi.org/https://doi.org/10.1111/nph.18129, 2022.

Deans, R. M., Meir, P., Dewar, R. C., and Mencuccini, M.: Evolutionary trade-offs under stochastic water stress shape xylem vulnerability to drought, Proceedings of the National Academy of Sciences, 123, e2516579 123, https://doi.org/10.1073/pnas.2516579123, 2026.

https://doi.org/10.5194/egusphere-2026-4729
Preprint. Discussion started: 31 August 2026

Dietrich, L., Delzon, S., Hoch, G., and Kahmen, A.: No role for xylem embolism or carbohydrate shortage in temperate trees during the severe 2015 drought, Journal of Ecology, 107, 334–349, https://doi.org/https://doi.org/10.1111/1365-2745.13051, 2019.

Dupuy, J.-l., Fargeon, H., Martin-StPaul, N., Pimont, F., Ruffault, J., Guijarro, M., Hernando, C., Madrigal, J., and Fernandes, P.: Climate Change Impact on Future Wildfire Danger and Activityin Southern Europe: A Review, https://doi.org/10.20944/preprints201910.0200.v1, 2019.

Eller, C. B., Rowland, L., Mencuccini, M., Rosas, T., Williams, K., Harper, A., Medlyn, B. E., Wagner, Y., Klein, T., Teodoro, G. S., Oliveira, R. S., Matos, I. S., Rosado, B. H. P., Fuchs, K., Wohlfahrt, G., Montagnani, L., Meir, P., Sitch, S., and Cox, P. M.: Stomatal optimization based on xylem hydraulics (SOX) improves land surface model simulation of vegetation responses to climate, New Phytologist, 226, 1622–1637, https://doi.org/https://doi.org/10.1111/nph.16419, 2020.

Farquhar, G., von Caemmerer, S., and Berry, J.: A biochemical model of photosynthetic CO, Planta, 149, 78–90, https://doi.org/10.1007/BF00386231, 1980.

Gentilesca, T., Camarero, J., Colangelo, M., Nole, A., and Ripullone, F.: Drought-induced oak decline in the western Mediterranean region: an overview on current evidences, mechanisms and management options to improve forest resilience, iForest - Biogeosciences and Forestry, 10, 796–806, https://doi.org/10.3832/ifor2317-010, 2017.

Guan, X., Werner, J., Cao, K.-F., Pereira, L., Kaack, L., McAdam, S. A. M., and Jansen, S.: Stem and leaf xylem of angiosperm trees experiences minimal embolism in temperate forests during two consecutive summers with moderate drought, Plant Biology, 24, 1208–1223, https://doi.org/https://doi.org/10.1111/plb.13384, 2022.

Hammond, W., Williams, A., Abatzoglou, J., Adams, H., Klein, T., López, R., Saenz-Romero, C., Hartmann, H., Breshears, D., and Allen, C.: Global field observations of tree die-off reveal hotter-drought fingerprint for Earth's forests, Nature Communications, 13, 1234567 890, https://doi.org/10.1038/s41467-022-29289-2, 2022.

Harper, A., Cox, P., Friedlingstein, P., Wiltshire, A., Jones, C., Sitch, S., Mercado, L., Groenendijk, M., Robertson, E., Kattge, J., Bönisch, G., Atkin, O., Bahn, M., Cornelissen, J., Niinemets, , Onipchenko, V., Penuelas, J., Poorter, L., Reich, P., and Bodegom, P.: Improved representation of plant functional types and physiology in the Joint UK Land Environment Simulator (JULES v4.2) using plant trait information, Geoscientific Model Development, 9, 2415–2440, https://doi.org/10.5194/gmd-9-2415-2016, 2016.

Hollis, D., McCarthy, M., Kendon, M., Legg, T., and Simpson, I.: HadUK-Grid—A new UK dataset of gridded climate observations, Geoscience Data Journal, 6, 151–159, https://doi.org/https://doi.org/10.1002/gdj3.78, 2019.

Huang, Y., Salama, M., Su, Z., van der Velde, R., Zheng, D., Krol, M., Hoekstra, A., and Zhou, Y.: Effects of Roughness Length Parameterizations on Regional-Scale Land Surface Modeling of Alpine Grasslands in the Yangtze River Basin, Journal of Hydrometeorology, 17, 1069–1085, https://doi.org/10.1175/JHM-D-15-0049.1, 2016.

Jiao, T., Williams, C. A., De Kauwe, M. G., Schwalm, C. R., and Medlyn, B. E.: Patterns of post-drought recovery are strongly influenced by drought duration, frequency, post-drought wetness, and bioclimatic setting, Global Change Biology, 27, 4630–4643, https://doi.org/https://doi.org/10.1111/gcb.15788, 2021.

Kannenberg, S. A., Novick, K. A., Alexander, M. R., Maxwell, J. T., Moore, D. J. P., Phillips, R. P., and Anderegg, W. R. L.: Linking drought legacy effects across scales: From leaves to tree rings to ecosystems, Global Change Biology, 25, 2978–2992, https://doi.org/https://doi.org/10.1111/gcb.14710, 2019.

KATTGE, J., KNORR, W., RADDATZ, T., and WIRTH, C.: Quantifying photosynthetic capacity and its relationship to leaf nitrogen content for global-scale terrestrial biosphere models, Global Change Biology, 15, 976–991, https://doi.org/https://doi.org/10.1111/j.1365-2486.2008.01744.x, 2009.

https://doi.org/10.5194/egusphere-2026-4729
Preprint. Discussion started: 31 August 2026

Kennedy, D., Swenson, S., Oleson, K. W., Lawrence, D. M., Fisher, R., Lola da Costa, A. C., and Gentine, P.: Implementing Plant Hydraulics in the Community Land Model, Version 5, Journal of Advances in Modeling Earth Systems, 11, 485–513, https://doi.org/https://doi.org/10.1029/2018MS001500, 2019.

Klein, T., Zeppel, M., Anderegg, W., Bloemen, J., De Kauwe, M., Hudson, P., Ruehr, N., Powell, T., von Arx, G., and Nardini, A.: Xylem embolism refilling and resilience against drought-induced mortality in woody plants: processes and trade-offs, Ecological Research, 33, https://doi.org/10.1007/s11284-018-1588-y, 2018.

Knutzen, F., Averbeck, P., Barrasso, C., Bouwer, L. M., Gardiner, B., Grünzweig, J. M., Hänel, S., Haustein, K., Johannessen, M. R., Kollet, S., Müller, M. M., Pietikäinen, J.-P., Pietras-Couffignal, K., Pinto, J. G., Rechid, D., Rousi, E., Russo, A., Suarez-Gutierrez, L., Veit, S., Wendler, J., Xoplaki, E., and Gliksman, D.: Impacts on and damage to European forests from the 2018–2022 heat and drought events, Natural Hazards and Earth System Sciences, 25, 77–117, https://doi.org/10.5194/nhess-25-77-2025, 2025.

Kolus, H., Huntzinger, D., Schwalm, C., Fisher, J., McKay, N., Fang, Y., Michalak, A., Schaefer, K., Wei, Y., Poulter, B., Mao, J., Parazoo, N., and Shi, X.: Land carbon models underestimate the severity and duration of drought's impact on plant productivity, Scientific Reports, 9, https://doi.org/10.1038/s41598-019-39373-1, 2019.

Lobo, A., Torres-Ruiz, J. M., Burlett, R., Lemaire, C., Parise, C., Francioni, C., Truffaut, L., Tomášková, I., Hansen, J. K., Kjær, E. D., Kremer, A., and Delzon, S.: Assessing inter- and intraspecific variability of xylem vulnerability to embolism in oaks, Forest Ecology and Management, 424, 53–61, https://doi.org/https://doi.org/10.1016/j.foreco.2018.04.031, 2018.

Lu, Y., Duursma, R. A., Farrior, C. E., Medlyn, B. E., and Feng, X.: Optimal stomatal drought response shaped by competition for water and hydraulic risk can explain plant trait covariation, New Phytologist, 225, 1206–1217, https://doi.org/https://doi.org/10.1111/nph.16207, 2020.

Mackay, D., Roberts, D., Ewers, B., Sperry, J., McDowell, N., and Pockman, W.: Interdependence of chronic hydraulic dysfunction and canopy processes can improve integrated models of tree response to drought, Water Resources Research, 51, https://doi.org/10.1002/2015WR017244, 2015.

Martin-StPaul, N. K., Limousin, J.-M., Vogt-Schilb, H., Rodríguez-Calcerrada, J., Rambal, S., Longepierre, D., and Misson, L.: The temporal response to drought in a Mediterranean evergreen tree: comparing a regional precipitation gradient and a throughfall exclusion experiment, Global Change Biology, 19, 2413–2426, https://doi.org/https://doi.org/10.1111/gcb.12215, 2013.

Mauna Loa Observatory: Dr. Xin Lan, NOAA/GML (gml.noaa.gov/ccgg/trends/) and Dr. Ralph Keeling, Scripps Institution of Oceanography (scrippsco2.ucsd.edu/).

McDowell, N., Pockman, W. T., Allen, C. D., Breshears, D. D., Cobb, N., Kolb, T., Plaut, J., Sperry, J., West, A., Williams, D. G., and Yepez, E. A.: Mechanisms of plant survival and mortality during drought: why do some plants survive while others succumb to drought?, New Phytologist, 178, 719–739, https://doi.org/https://doi.org/10.1111/j.1469-8137.2008.02436.x, 2008.

McDowell, N., Sapes, G., Pivovaroff, A., Adams, H., Allen, C., Anderegg, W., Arend, M., Breshears, D., Brodribb, T., Choat, B., Cochard, H., De Cáceres, M., De Kauwe, M., Grossiord, C., Hammond, W., Hartmann, H., Hoch, G., Kahmen, A., Klein, T., and Xu, C.: Mechanisms of woody-plant mortality under rising drought, CO2 and vapour pressure deficit, Nature Reviews Earth Environment, 3, 1–15, https://doi.org/10.1038/s43017-022-00272-1, 2022.

MEDLYN, B. E., DUURSMA, R. A., EAMUS, D., ELLSWORTH, D. S., PRENTICE, I. C., BARTON, C. V. M., CROUS, K. Y., DE ANGELIS, P., FREEMAN, M., and WINGATE, L.: Reconciling the optimal and empirical approaches to modelling stomatal conductance, Global Change Biology, 17, 2134–2144, https://doi.org/https://doi.org/10.1111/j.1365-2486.2010.02375.x, 2011.

https://doi.org/10.5194/egusphere-2026-4729
Preprint. Discussion started: 31 August 2026

Myneni, R., Knyazikhin, Y., and Park, T.: MODIS/Terra+Aqua Leaf Area Index/FPAR 4-Day L4 Global 500m SIN Grid V061, https://doi.org/doi.org/10.5067/MODIS/MCD15A3H.061, 2021.

Nakhavali, M. A., Lauerwald, R., Regnier, P., Guenet, B., Chadburn, S., and Friedlingstein, P.: Leaching of dissolved organic carbon from mineral soils plays a significant role in the terrestrial carbon balance, Global Change Biology, https://doi.org/10.1111/gcb.15460, 2020.

Oberleitner, F., Hartmann, H., Hasibeder, R., Huang, J., Losso, A., Mayr, S., Oberhuber, W., Wieser, G., and Bahn, M.: Amplifying effects of recurrent drought on the dynamics of tree growth and water use in a subalpine forest, Plant, Cell & Environment, 45, 2617–2635, https://doi.org/https://doi.org/10.1111/pce.14369, 2022.

Ogaya, R. and Penuelas, J.: Contrasting foliar responses to drought in Quercus ilex and Phillyrea latifolia, Biologia plantarum, 50, 373–382, 2006.

Ogle, K., Barber, J. J., Barron-Gafford, G. A., Bentley, L. P., Young, J. M., Huxman, T. E., Loik, M. E., and Tissue, D. T.: Quantifying ecological memory in plant and ecosystem processes, Ecology Letters, 18, 221–235, https://doi.org/https://doi.org/10.1111/ele.12399, 2015.

Paschalis, A., De Kauwe, M. G., Sabot, M., and Fatichi, S.: When do plant hydraulics matter in terrestrial biosphere modelling?, Global Change Biology, 30, e17 022, https://doi.org/https://doi.org/10.1111/gcb.17022, e17022 GCB-23-2221, 2024.

Ramírez-Valiente, J., Poyatos, R., Blackman, C., Cabon, A., Castells, E., Cochard, H., Creek, D., Delzon, S., García-Valdés, R., Limousin, J.-M., López, R., Martin-StPaul, N., Moreno, M., Rowland, L., Santiago, L., Schuldt, B., Torres-Ruiz, J. M., Valade, A., Martinez Vilalta, J., and Mencuccini, M.: Limited plastic responses in safety traits support greater hydraulic risk under drier conditions, Nature Ecology Evolution, 9, 1825–1836, https://doi.org/10.1038/s41559-025-02830-4, 2025.

Rao, M. P., Pacheco-Solana, A., Li, R., Oryan, B., Jensen, J. E., Rodriguez-Caton, M., Klinek, L., Pierrat, Z. A., Ruehr, S., Oelkers, R., Boeschoten, L. E., Griffin, K. L., McCormack, M. L., Yang, X., Verfaillie, J., Baldocchi, D., Hise, J., Turner, A. J., Scanlon, T. M., Andreu-Hayles, L., Eitel, J. U. H., Pederson, N., Griffin, D., Stahle, D., Maxwell, J. T., Voelker, S., Kannenberg, S. A., Peñuelas, J., and Magney, T. S.: Decoupled carbon assimilation and growth responses to aridity in temperate deciduous oaks, Science Advances, 12, eady7139, https://doi.org/10.1126/sciadv.ady7139, 2026.

Reyer, C. P. O., Brouwers, N., Rammig, A., Brook, B. W., Epila, J., Grant, R. F., Holmgren, M., Langerwisch, F., Leuzinger, S., Lucht, W., Medlyn, B., Pfeifer, M., Steinkamp, J., Vanderwel, M. C., Verbeeck, H., and Villela, D. M.: Forest resilience and tipping points at different spatio-temporal scales: approaches and challenges, Journal of Ecology, 103, 5–15, https://doi.org/https://doi.org/10.1111/1365-2745.12337, 2015.

Ruehr, N., Grote, R., Mayr, S., and Arneth, A.: Beyond the extreme: recovery of carbon and water relations in woody plants following heat and drought stress, Tree Physiology, 39, 1285–1299, https://doi.org/10.1093/treephys/tpz032, 2019.

Ruffault, J., Pimont, F., Cochard, H., Dupuy, J.-l., and Martin-StPaul, N.: SurEau-Ecos v2.0: A trait-based plant hydraulics model for simulations of plant water status and drought-induced mortality at the ecosystem level, https://doi.org/10.5194/gmd-2022-17, 2022.

Sabot, M., De Kauwe, M., Pitman, A., Medlyn, B., Ellsworth, D., Martin-StPaul, N., Wu, J., Choat, B., Limousin, J., Mitchell, P., Rogers, A., and Serbin, S.: One Stomatal Model to Rule Them All? Toward Improved Representation of Carbon and Water Exchange in Global Models, Journal of Advances in Modeling Earth Systems, 14, https://doi.org/10.1029/2021MS002761, 2022a.

Sabot, M. E. B., De Kauwe, M. G., Pitman, A. J., Medlyn, B. E., Verhoef, A., Ukkola, A. M., and Abramowitz, G.: Plant profit maximization improves predictions of European forest responses to drought, New Phytologist, 226, 1638–1655, https://doi.org/https://doi.org/10.1111/nph.16376, 2020.

https://doi.org/10.5194/egusphere-2026-4729
Preprint. Discussion started: 31 August 2026

Sabot, M. E. B., De Kauwe, M. G., Pitman, A. J., Ellsworth, D. S., Medlyn, B. E., Caldararu, S., Zaehle, S., Crous, K. Y., Gimeno, T. E., Wujeska-Klause, A., Mu, M., and Yang, J.: Predicting resilience through the lens of competing adjustments to vegetation function, Plant, Cell & Environment, 45, 2744–2761, https://doi.org/https://doi.org/10.1111/pce.14376, 2022b.

Schneider, M. and Goss, K.-U.: Prediction of the water sorption isotherm in air dry soils, Geoderma, 170, 64–69, https://doi.org/https://doi.org/10.1016/j.geoderma.2011.10.008, 2012.

Schuldt, B., Buras, A., Arend, M., Vitasse, Y., Beierkuhnlein, C., Damm, A., Gharun, M., Grams, T. E., Hauck, M., Hajek, P., Hartmann, H., Hiltbrunner, E., Hoch, G., Holloway-Phillips, M., Körner, C., Larysch, E., Lübbe, T., Nelson, D. B., Rammig, A., Rigling, A., Rose, L., Ruehr, N. K., Schumann, K., Weiser, F., Werner, C., Wohlgemuth, T., Zang, C. S., and Kahmen, A.: A first assessment of the impact of the extreme 2018 summer drought on Central European forests, Basic and Applied Ecology, 45, 86–103, https://doi.org/https://doi.org/10.1016/j.baae.2020.04.003, 2020.

Schwalm, C. R., Anderegg, W. R. L., Michalak, A. M., Fisher, J. B., Biondi, F., Koch, G., Litvak, M., Ogle, K., Shaw, J. D., Wolf, A., Huntzinger, D. N., Schaefer, K., Cook, R., Wei, Y., Fang, Y., Hayes, D., Huang, M., Jain, A., and Tian, H.: Global patterns of drought recovery, Nature, 548, 202–205, https://doi.org/10.1038/nature23021, 2017.

Schönbeck, L. C., Schuler, P., Lehmann, M. M., Mas, E., Mekarni, L., Pivovaroff, A. L., Turberg, P., and Grossiord, C.: Increasing temperature and vapour pressure deficit lead to hydraulic damages in the absence of soil drought, Plant, Cell & Environment, 45, 3275–3289, https://doi.org/https://doi.org/10.1111/pce.14425, 2022.

Seneviratne, S. and Ciais, P.: Environmental science: Trends in ecosystem recovery from drought, Nature, 548, 164–165, https://doi.org/10.1038/548164a, 2017.

Shao, X., Zhang, Y., Zhang, X., Tian, J., Xu, Z., and Liu, C.: Drought-induced ecosystem resistance and recovery observed at 118 flux tower stations across the globe, Agricultural and Forest Meteorology, 356, 110 170, https://doi.org/10.1016/j.agrformet.2024.110170, 2024.

Sinacore, K., Asbjornsen, H., Hernandez-Santana, V., and Hall, J. S.: Drought Differentially Affects Growth, Transpiration, and Water Use Efficiency of Mixed and Monospecific Planted Forests, Forests, 10, https://doi.org/10.3390/f10020153, 2019.

Sperry, J. S., Venturas, M. D., Anderegg, W. R. L., Mencuccini, M., Mackay, D. S., Wang, Y., and Love, D. M.: Predicting stomatal responses to the environment from the optimization of photosynthetic gain and hydraulic cost, Plant, Cell & Environment, 40, 816–830, https://doi.org/https://doi.org/10.1111/pce.12852, 2017.

Sulman, B. N., Roman, D. T., Yi, K., Wang, L., Phillips, R. P., and Novick, K. A.: High atmospheric demand for water can limit forest carbon uptake and transpiration as severely as dry soil, Geophysical Research Letters, 43, 9686–9695, https://doi.org/https://doi.org/10.1002/2016GL069416, 2016.

Tripathy, K. P. and Mishra, A. K.: How unusual is the 2022 European compound drought and heatwave event?, Geophysical Research Letters, 50, e2023GL105 453, 2023.

Trugman, A., detto, M., Bartlett, M., Medvigy, D., Anderegg, W., Schwalm, C., Schaffer, B., and Pacala, S.: Tree carbon allocation explains forest drought-kill and recovery patterns, Ecology Letters, 21, https://doi.org/10.1111/ele.13136, 2018.

Ukkola, A., De Kauwe, M., Pitman, A., Best, M., Abramowitz, G., Haverd, V., Decker, M., and Haughton, N.: Land surface models systematically overestimate the intensity, duration and magnitude of seasonal-scale evaporative droughts, Environmental Research Letters, 11, 104 012, https://doi.org/10.1088/1748-9326/11/10/104012, 2016.

Urli, M., Lamy, J.-B., Fabrice, S., Burlett, R., Sylvain, D., and Porté, A.: The high vulnerability of Quercus robur to drought at its southern margin paves the way for Quercus ilex, Plant Ecology, 216, https://doi.org/10.1007/s11258-014-0426-8, 2014.

https://doi.org/10.5194/egusphere-2026-4729
Preprint. Discussion started: 31 August 2026

Vicente-Serrano, S., Beguería, S., and López-Moreno, J.: A Multiscalar Drought Index Sensitive to Global Warming: The Standardized Precipitation Evapotranspiration Index, Journal of Climate, 23, 1696–1718, https://doi.org/10.1175/2009JCLI2909.1, 2010.

Webb, S. W.: A simple extension of two-phase characteristic curves to include the dry region, Water Resources Research, 36, 1425–1430, https://doi.org/https://doi.org/10.1029/2000WR900057, 2000.

Werner, C., Bahn, M., Grams, T., Grossiord, C., Haberstroh, S., Lenczner, G., Tuia, D., and Vallicrosa, H.: Impact of emerging compound droughts on forests: A water supply and demand perspective, Plant Biology, https://doi.org/10.1111/plb.70080, 2025.

Wilkinson, M., Eaton, E. L., Broadmeadow, M. S. J., and Morison, J. I. L.: Inter-annual variation of carbon uptake by a plantation oak woodland in south-eastern England, Biogeosciences, 9, 5373–5389, https://doi.org/10.5194/bg-9-5373-2012, 2012.

Wolfe, B. T., Sperry, J. S., and Kursar, T. A.: Does leaf shedding protect stems from cavitation during seasonal droughts? A test of the hydraulic fuse hypothesis, New Phytologist, 212, 1007–1018, https://doi.org/https://doi.org/10.1111/nph.14087, 2016.

Wright, I. J., Reich, P. B., Cornelissen, J. H. C., Falster, D. S., Garnier, E., Hikosaka, K., Lamont, B. B., Lee, W., Oleksyn, J., Osada, N., Poorter, H., Villar, R., Warton, D. I., and Westoby, M.: Assessing the generality of global leaf trait relationships, New Phytologist, 166, 485–496, https://doi.org/https://doi.org/10.1111/j.1469-8137.2005.01349.x, 2005.

Yao, Y., Wang, Y., Yin, Y., Wood, J. D., and Frankenberg, C.: Improved model predictions of carbon and water fluxes by including drought legacy effects, EGUsphere, 2025, 1–22, https://doi.org/10.5194/egusphere-2025-5684, 2025.

Yu, Z., Wang, J., Liu, S., Rentch, J., Sun, P., and Lu, C.: Global gross primary productivity and water use efficiency changes under drought stress, Environmental Research Letters, 12, 014 016, https://doi.org/10.1088/1748-9326/aa5258, 2017.

Zhao, H., Luo, R., Cai, J., Wang, Y., Luo, F., Li, L., Liu, H., and Li, S.: Coupled allometric scaling in biomass allocation and hydraulic resistance partitioning sustains water homeostasis throughout ontogeny, New Phytologist, n/a, https://doi.org/https://doi.org/10.1111/nph.71245, 2026.

https://doi.org/10.5194/egusphere-2026-4729
Preprint. Discussion started: 31 August 2026

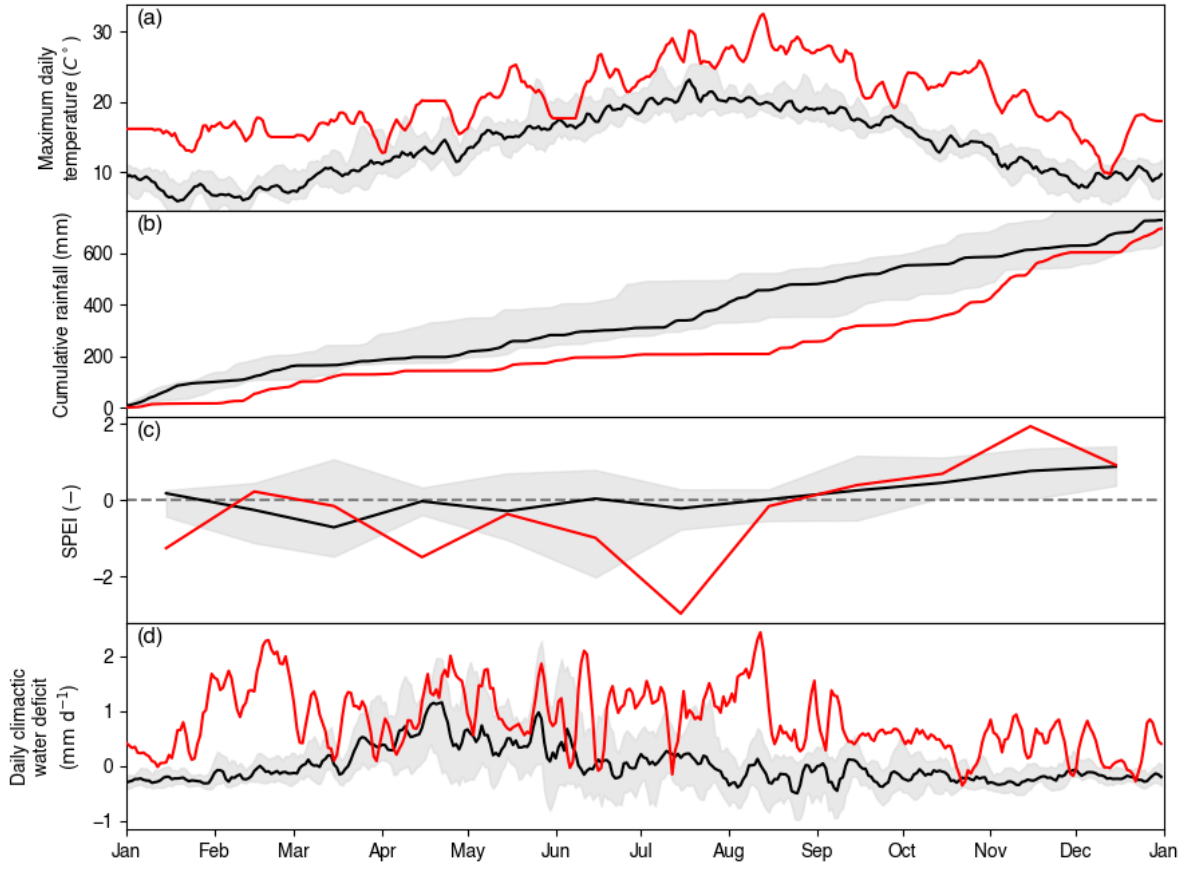

Figure 1. Observed maximum daily temperature (a), cumulative rainfall (b), monthly Standardised Precipitation-Evapotranspiration Index (c, Vicente-Serrano et al., 2010) and cumulative water deficit (d) for the year 2022 (red) compared to the average over the period 1999 to 2019 (black) The shaded grey region indicates one standard deviation from the average for the period 1999 to 2019.

https://doi.org/10.5194/egusphere-2026-4729
Preprint. Discussion started: 31 August 2026

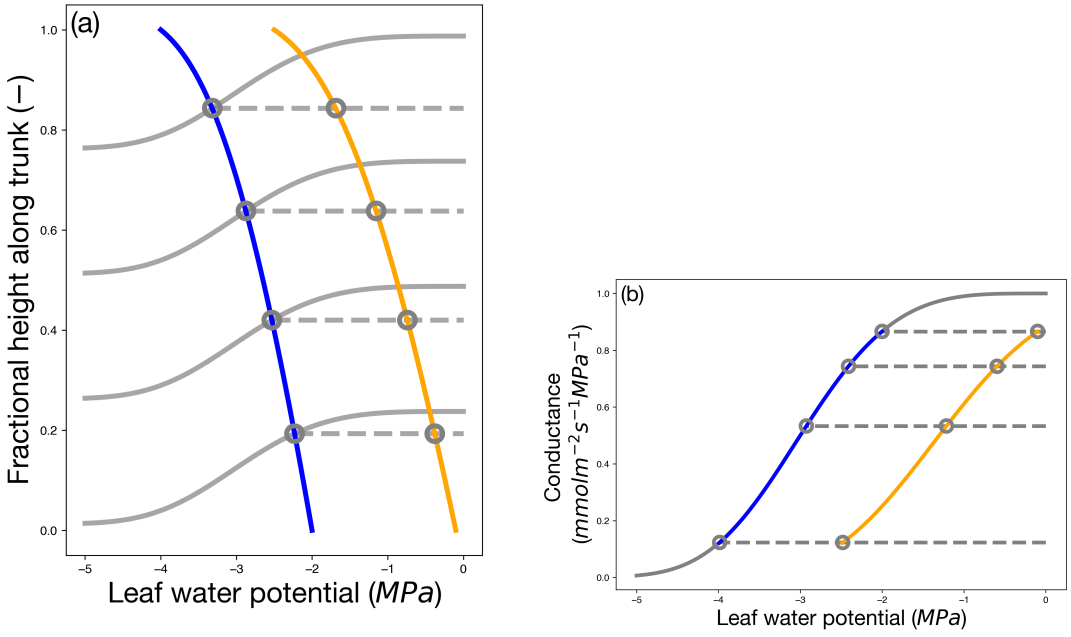

Figure 2. Schematic depicting the whole trunk impairment model Panel a depicts water potential along the height of the trunk under the historic extreme (minimum) water potential (blue) and the impaired water potential (orange) The unimpaired vulnerability curve (solid grey line) and impaired vulnerability curve (dashed grey line) depict conductance at four different heights along the trunk Panel b depicts the historic extreme (minimum) water potential conductance curve (blue) and the impaired curve (orange) for the leaf and root water potentials shown in the left panel The unimpaired vulnerability curve is shown as a solid grey line The impaired vulnerability curve at four different heights is shown by the dashed grey line.

https://doi.org/10.5194/egusphere-2026-4729
Preprint. Discussion started: 31 August 2026

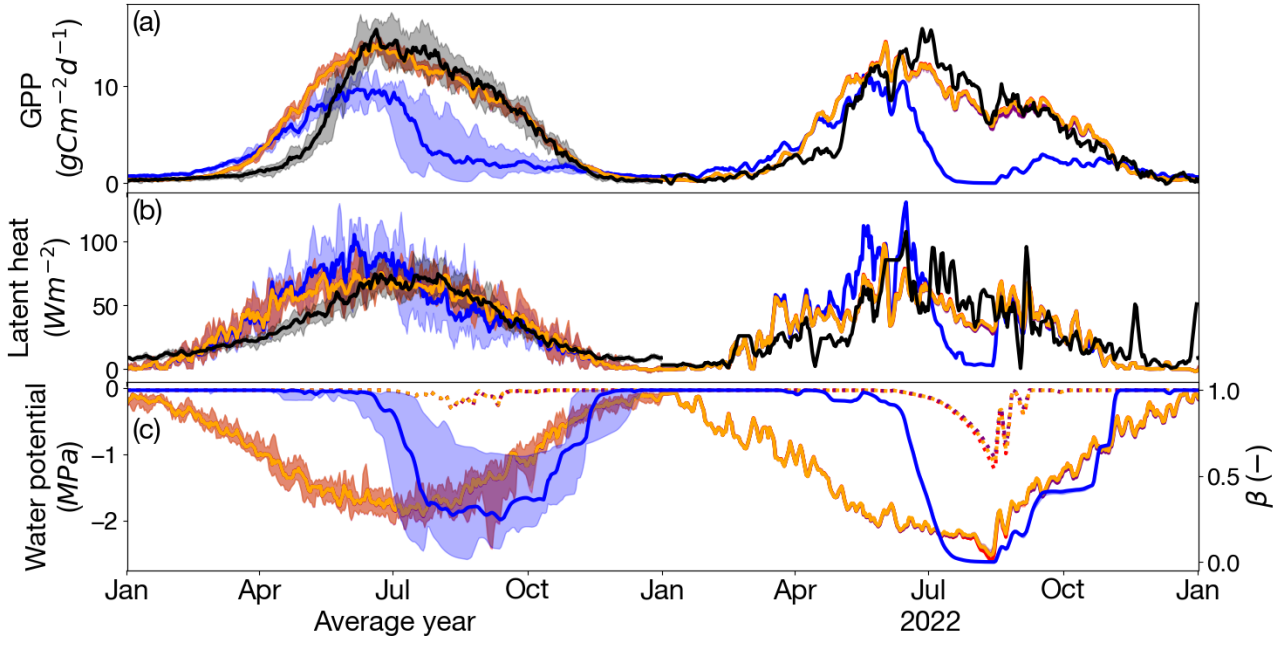

Figure 3. Predicted grose Primary Productivity (a), and latent energy flux (b) for an average year (2011 to 2017, inclusive) and the 2022 drought year Predictions for the CTRL, Profit-Max, kmax impairment and whole trunk impairment models, are shown in blue, red, purple and orange, with observed GPP and Latent heat in black The Profit-Max (red) and k_{max}-impaired (purple) models tend to be obscured by the whole trunk impairment model (orange) Shaded regions indicate one standard deviation across the ensemble Panel c shows the fractional soil moisture content for the CTRL model as a solid blue line Panel c also shows mid day leaf and root zone water potentials as a solid and dashed line respectively for models other than the CTRL model.

https://doi.org/10.5194/egusphere-2026-4729
Preprint. Discussion started: 31 August 2026

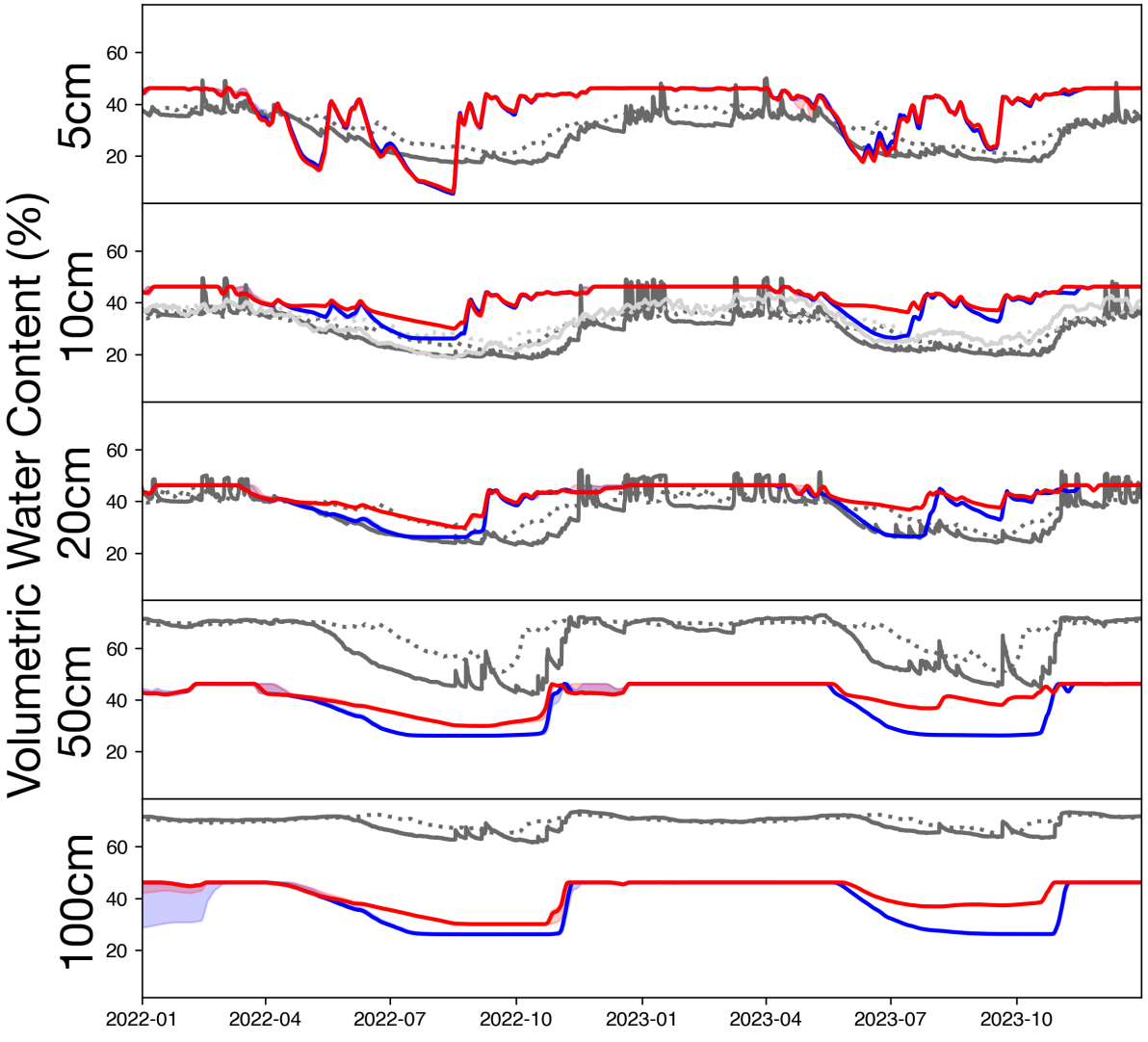

Figure 4. Volumetric soil water content measured at multiple depths (5cm, 10cm, 20cm, 50cm and 100cm from top down). Observations of volumetric soil moisture content using CS616 sensors (Campbell Scientific, Shepshed, UK) and from the Cosmic-ray soil moisture monitoring network UK data base (Cooper et al., 2021) are plotted as a solid dark and light grey line respectively. The dotted lines show observed volumetric soil water content during an average year. Predicted volumetric soil water content by the Ctrl and profit-max model are plotted in blue and red respectivly.

https://doi.org/10.5194/egusphere-2026-4729
Preprint. Discussion started: 31 August 2026

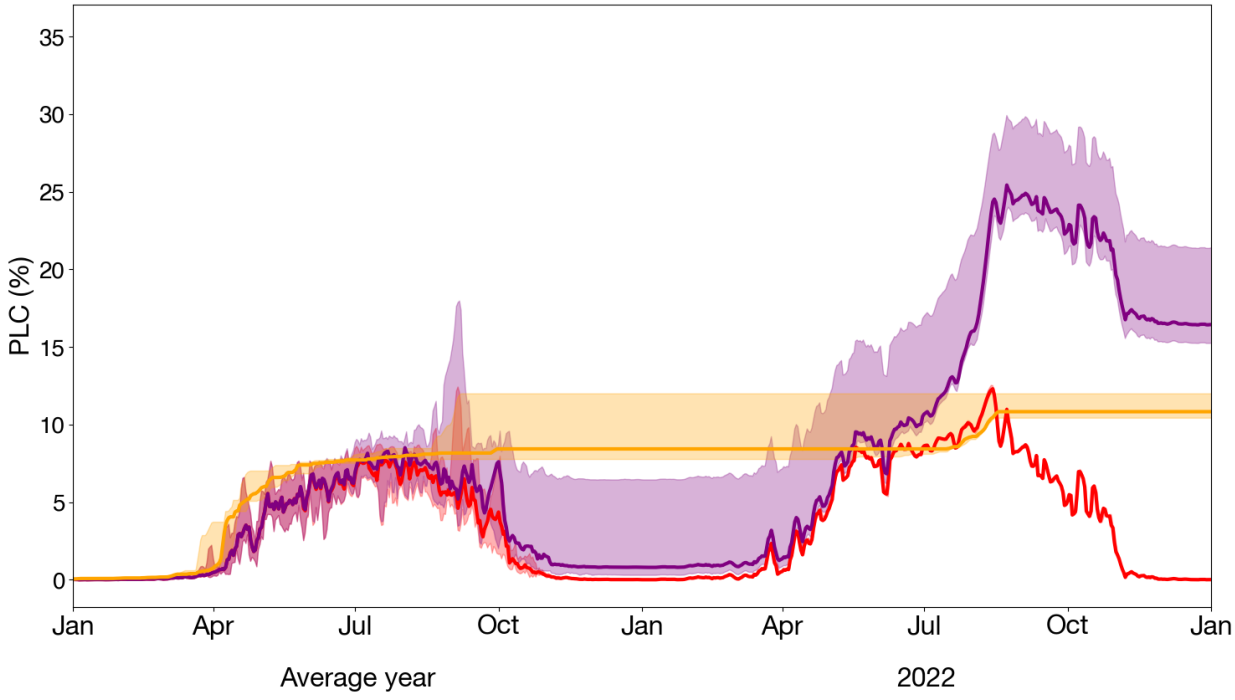

Figure 5. Predicted percentage loss of conductance in the leaf by the Profit-Max (red), k_{max}-impaired (purple) and whole trunk impairment (orange) models during an average year and the 2022 drought year Shaded regions indicate one standard deviation across the ensemble of average years.

https://doi.org/10.5194/egusphere-2026-4729
Preprint. Discussion started: 31 August 2026

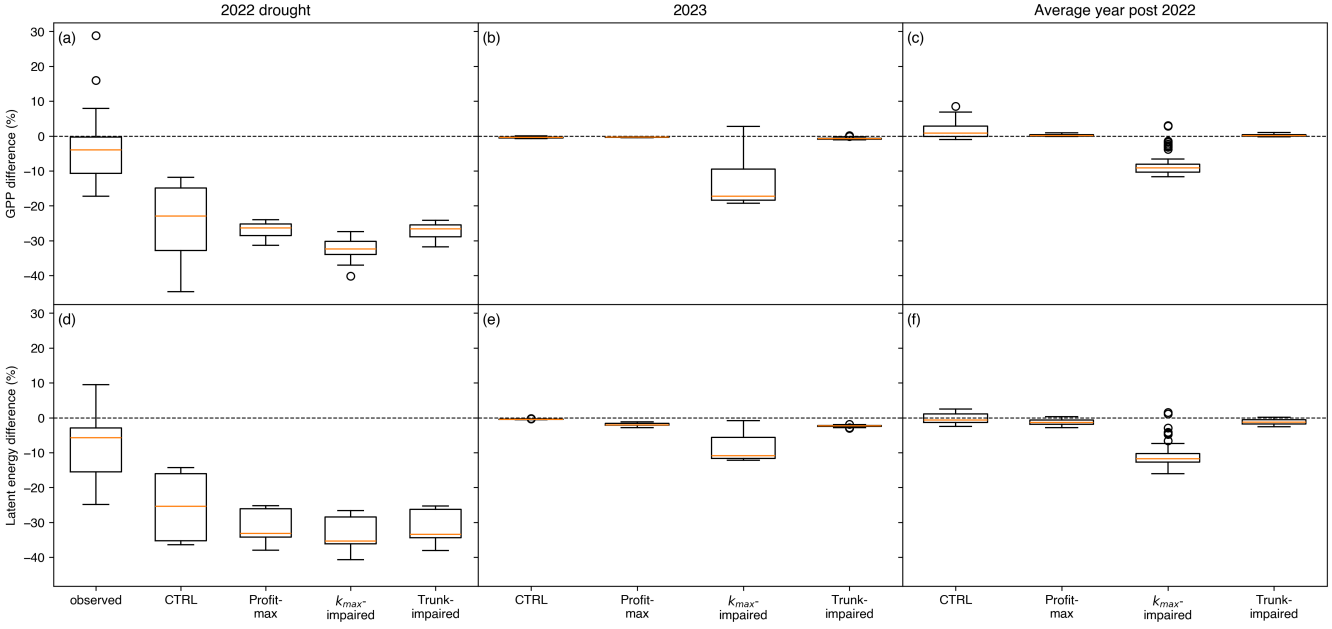

Figure 6. Percentage difference in GPP (a) and Latent energy (d) for the 2022 drought year compared to an average year. Percentage difference in GPP (b) and Latent energy (e) for 2023 compared to 2023 following another average year. Percentage difference in GPP (c) and Latent energy (f) for an average year following 2022 compared to an average year following another average year. Zero percentage difference is indicated by a dashed black line.

https://doi.org/10.5194/egusphere-2026-4729
Preprint. Discussion started: 31 August 2026

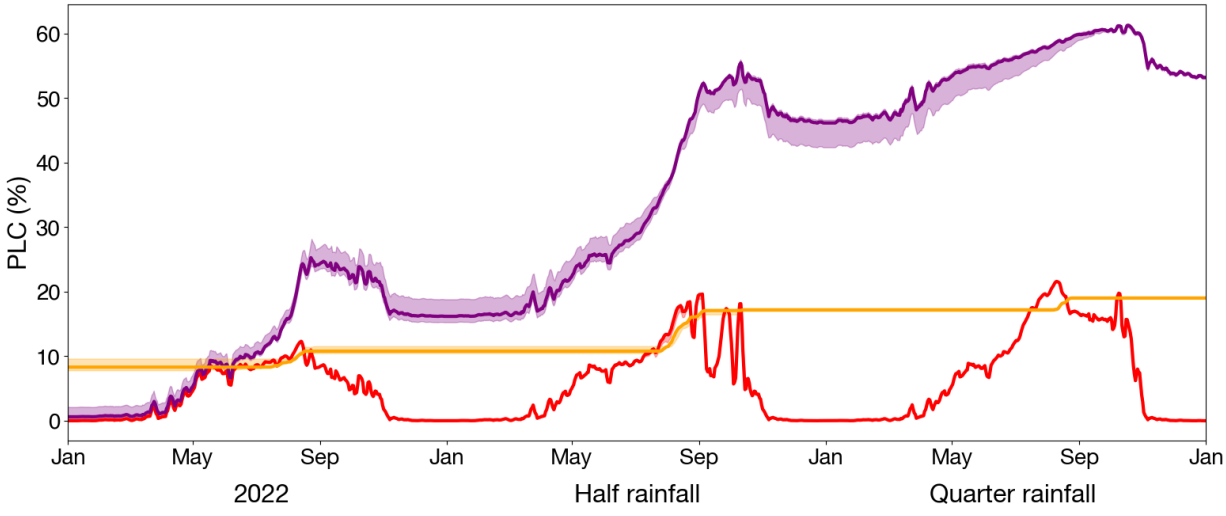

Figure 7. Percentage loss of conductivity at the ψ_l predicted by the Profit-Max (red), k_{max}-impaired (purple) and whole trunk impairment (orange) models during the 2022 drought year, 2022 with half rainfall and no spring rainfall, and 2022 with a quarter rainfall and no spring rainfall respectivly

https://doi.org/10.5194/egusphere-2026-4729
Preprint. Discussion started: 31 August 2026

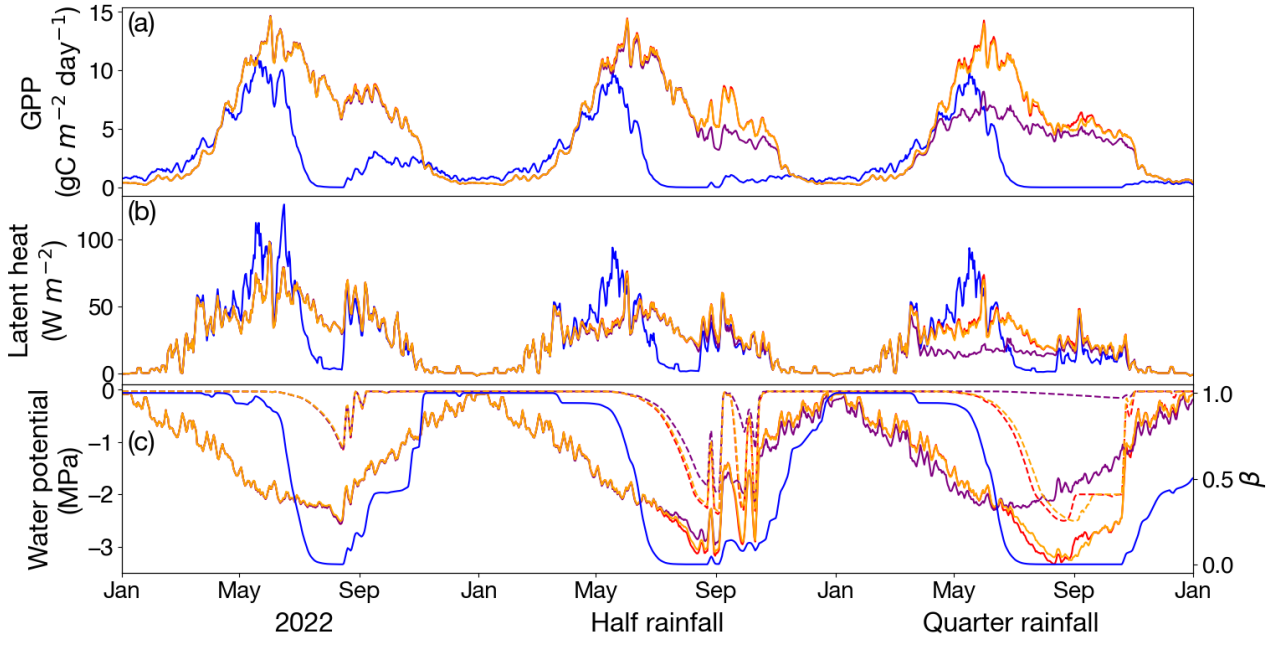

Figure 8. Predicted grose Primary Productivity (a), and latent energy flux (b) for the 2022 drought year, 2022 with half rainfall and no spring rainfall, and 2022 with a quarter rainfall and no spring rainfall The CTRL, Profit-Max, kmax impairment and whole trunk impairment model predictions are shown in blue, red, purple and orange respectively Panel c shows the fractional soil moisture content for the CTRL model as a solid blue line Panel c also shows midday leaf and root zone water potentials as a solid and dashed line respectively for models other than the CTRL model As in Fig. 3, the Profit-Max (red) and $k_{max} impairment (purple) model predictions are often obsscured by the whole trunk impairment model prediction.

https://doi.org/10.5194/egusphere-2026-4729
Preprint. Discussion started: 31 August 2026

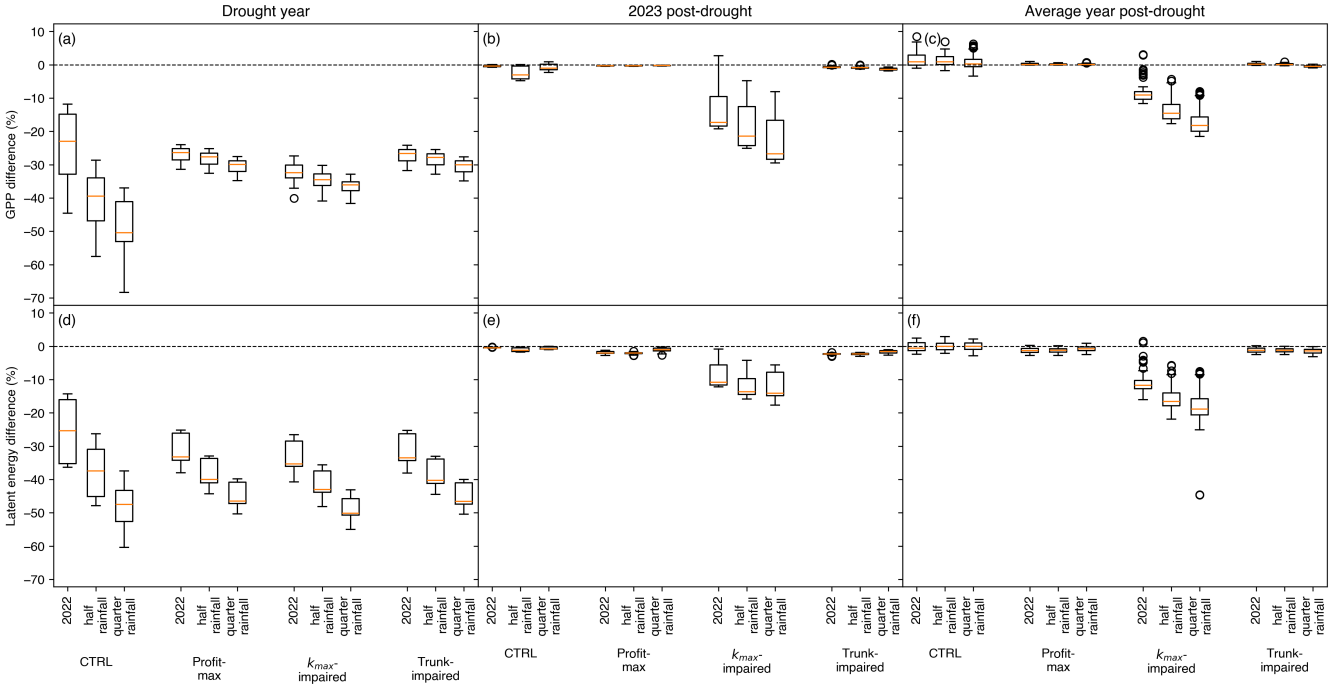

Figure 9. Predicted percentage difference in GPP (a) and leatent heat (d) between each drought scenario and an average year Predicted difference in GPP (b) and LE (e) between 2023 preceded by each drought scenario and 2023 preceded by an average year. Predicted difference in GPP (c) and LE (f) between an average year preceded by each drought scenario and an average year preceded by another average year. For each model the three drought scenarios are, left to right, the 2022 drought year, 2022 with half rainfall and no spring rainfall, and 2022 with a quarter rainfall and no spring rainfall.

https://doi.org/10.5194/egusphere-2026-4729
Preprint. Discussion started: 31 August 2026

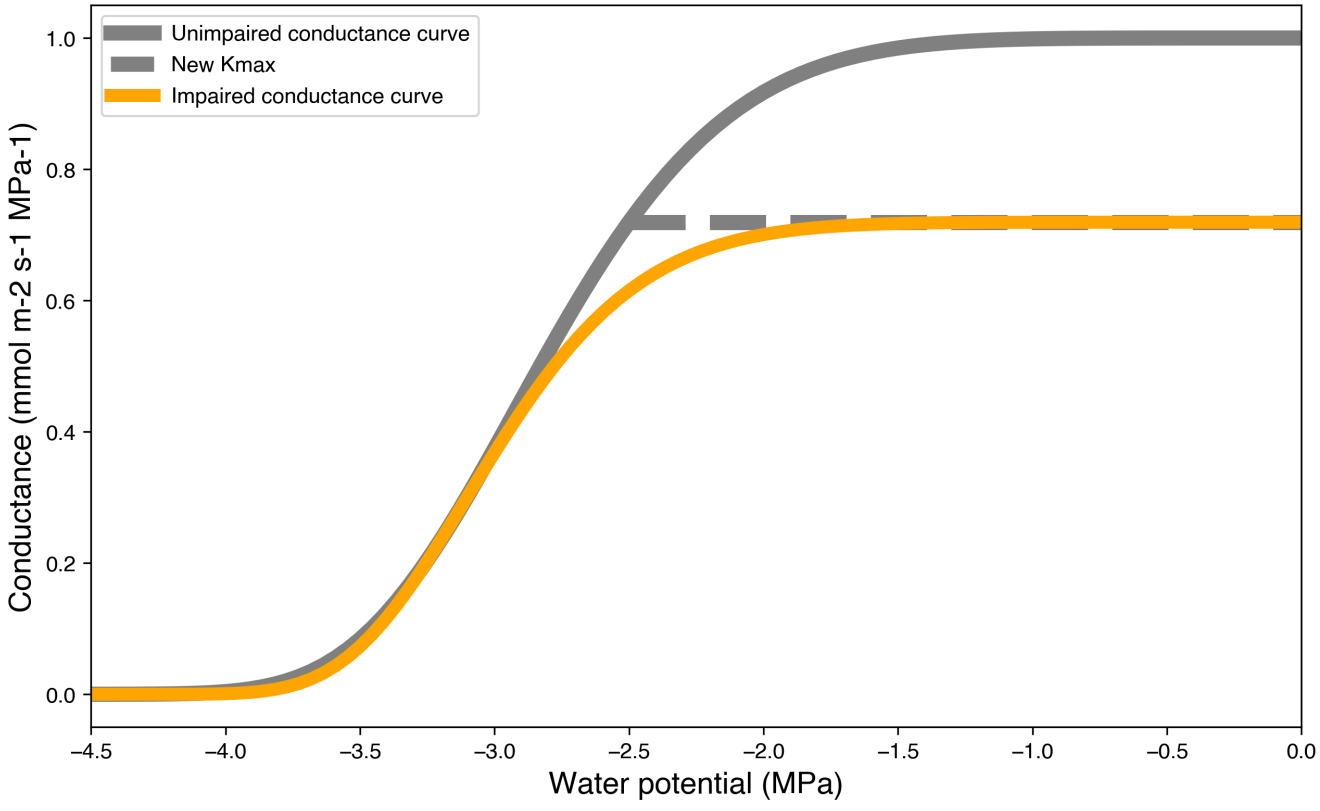

Figure A1. k_{max}-impaired model schematic. The new impaired hydraulic vulnerability curve (solid orange line) is shown compared to the unimpaired vulnerability curve (solid grey line) and the new maximum conductance (dashed grey line).

https://doi.org/10.5194/egusphere-2026-4729
Preprint. Discussion started: 31 August 2026

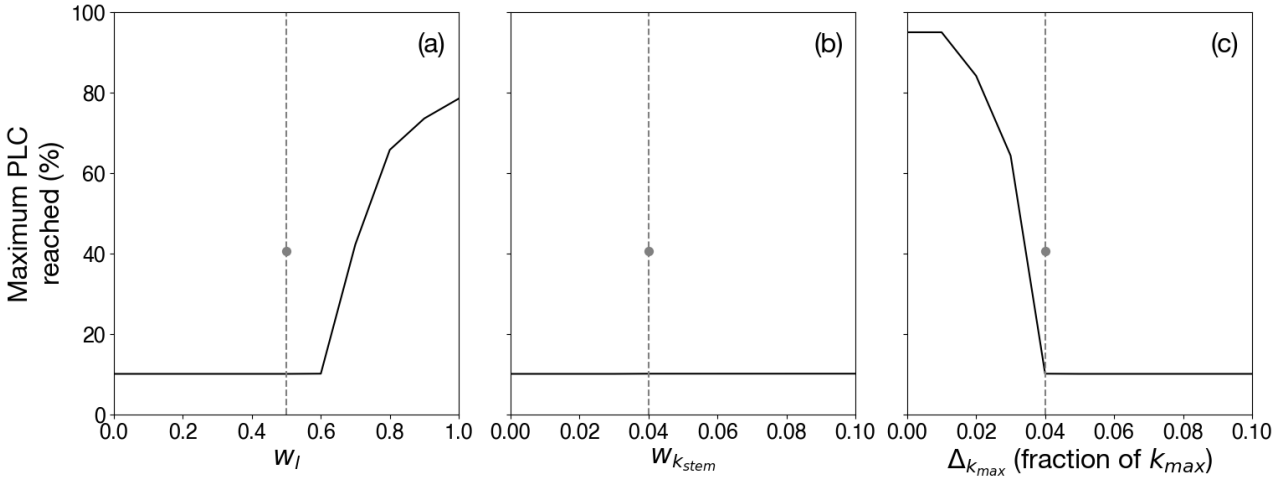

Figure A2. Simulated maximum PLC reached during 2022 (subplots a, b, and c) and PLC at the end of 2022 (subplots d, e, and f) as a function of each k_{max} impairment model parameter, w_l (subplots a, and d), $w_{k_{stem}}$ (subplots b, and e) and Δk_{max} (subplots c, and f). The median PLC (solid black line) and one standard deviation (shaded grey area) were calculated for each parameter by averaging across the two non-varying parameters.